



A T-MATRIX PERTURBATION FORMALISM FOR SCATTERING FROM A ROUGH FLUID-ELASTIC INTERFACE

G. C. BISHOP

Naval Undersea Warfare Center Division Newport, Newport, RI 02840, U.S.A.

(Received 19 September 1997, and in final form 30 April 1998)

A perturbative representation of the null field T-matrix for scattering a pressure wave from a fluid–elastic interface with surface roughness is developed. It is shown that the n th order T-matrix may be calculated recursively and expressed in terms of the elements of a zeroth order T-matrix. Further, it is shown that the expression for the n th order T-matrix is general in form and may be specialized to scattering from rigid and soft rough surfaces and from the rough surface of a fluid sediment. The T-matrix for the n th order spectral amplitude of the scattered pressure field in the fluid is calculated and its diagrammatic representation is constructed. For sinusoidal surface roughness, the perturbative representation of the T-matrix is used to calculate the spectral amplitudes of the Floquet modes of the pressure field scattered in the fluid. The results are compared with those obtained from a non-perturbative representation of the T-matrix and the accuracy and region of applicability of the formalism is determined. Then the relative scattering amplitudes of some of the individual scattering processes that occur in the diagrammatic representation of the T-matrix are calculated through second order. It is shown that diagrams that correspond to scalar processes in which surface pressure fields are excited and propagated tend to dominate diagrams that correspond to vector and tensor processes in which surface displacement fields are excited and propagated. A “scalar” approximation to the perturbation series is defined in which only scalar diagrams in the perturbation series are maintained. Numerical results for the perturbation series in the scalar approximation to fourth order are compared with exact results and it is shown that the scalar approximation provides reasonably accurate results for some applications.

1. INTRODUCTION

In this paper, a perturbative representation of the null field T-matrix for scattering a pressure wave from a rough fluid–elastic interface is derived. Although perturbative representations of the null field T-matrix for scattering from a fluid–elastic interface with surface roughness have been derived previously [1–3], the form of the T-matrix derived in this paper is somewhat different. The canonical form of the null field T-matrix avoids some of the formal and numerical difficulties that occur in formalisms based on surface field integral equations, is numerically robust, and has been widely used. However, since it is expressed as the product of the matrix of coefficients of the scattered field equations and the matrix solution

to the null field equations, it is somewhat problematic to construct a representation of the T-matrix in terms of physically meaningful vertices, propagators and intermediate fields that leads to a simple and intuitive diagrammatic representation that reveals much of the physics of the scattering process as is often done with iterated integral equation formalisms. From a computational point of view, the fact that the T-matrix does not render the physics of the scattering process transparent is not relevant and often is not considered. The perturbative representation of the null field T-matrix developed in this paper is both computationally tractable and physically intuitive. It is shown that the T-matrix can be expressed in terms of vertices and propagators and that this representation leads to simple diagrammatic rules, to a diagrammatic representation that reveals much of the physics, and provides an intuitive understanding of the scattering process. Alternatively, the diagrammatic rules can be used to obtain an analytic expression for the T-matrix at any order of perturbation theory or for any component scattering process from its diagrammatic representation. Expressions of the latter type can be used to determine the scattering amplitudes of the various scattering processes that contribute to the total scattering amplitude.

The T-matrix formalism is similar to that developed by Waterman [4–6], however, rather than spherical or cylindrical vector basis functions, rectangular scalar and vector basis functions that are more appropriate for scattering from non-isotropic non-periodic surface roughness are constructed from Weyl plane waves and used to represent vector and tensor fields. These vector functions admit a representation of the scattered displacement field in the elastic solid that is the sum of three vector fields; a longitudinally polarized p -wave field and two transversely polarized s -wave fields (i.e., SH and SV fields). Once the formalism for the rectangular vector functions is developed, this representation is considerably more convenient than a representation of the displacement field in terms of its rectangular components or in terms of spherical or cylindrical vector basis functions. Perturbative representations of matrix elements and fields are constructed and the problem is reduced to the calculation of the displacement and pressure field spectral amplitudes for an arbitrary order of the perturbation series.

It is assumed that a stationary source is located in a fluid half space above the rough surface of an elastic solid half space and is the origin of an acoustic pressure wave $p^{(0)}(\mathbf{r}, t)$ that is incident on and is scattered from the rough surface. The surface of the elastic solid is given by $z' = \xi(x', y')$ where $\xi(x', y')$ is the roughness profile function. Further, it is assumed that $\xi(x', y')$ is arbitrary and that there exists surface heights $h_1 = \max[\xi(x', y')]$, $h_2 = \min[\xi(x', y')]$ and $h = \max(|h_1|, |h_2|)$ so that $-h \leq h_2 \leq \xi(x', y') \leq h_1 \leq h$. It is assumed that the fluid and elastic media are homogeneous and isotropic and that the Lamé parameters and mass density are, respectively, $\lambda^{(1)}$ and $\rho^{(1)}$ for the fluid and $\lambda^{(2)}$, $\mu^{(2)}$ and $\rho^{(2)}$ for the elastic solid. The phase speed and wave number in the fluid are, respectively, $c_p^{(1)} = \sqrt{\lambda^{(1)}/\rho^{(1)}}$ and $k_p^{(1)} = \omega/c_p^{(1)}$. In the solid, the phase speed and wave number are, respectively, $c_s^{(2)} = \sqrt{\mu^{(2)}/\rho^{(2)}}$ and $k_s^{(2)} = \omega/c_s^{(2)}$ for s -waves and $c_p^{(2)} = \sqrt{(\lambda^{(2)} + 2\mu^{(2)})/\rho^{(2)}}$ and $k_p^{(2)} = \omega/c_p^{(2)}$ for p -waves. The superscripts (1) and (2) in these expressions and in all subsequent expressions are used, respectively, to designate quantities in the fluid

and the solid. It is assumed that all fields are time harmonic and that an arbitrary field may be expressed in the form $\psi(\mathbf{r}, t) = \psi(\mathbf{r}) e^{-i\omega t}$. However, the time dependent factor $e^{-i\omega t}$ and explicit dependence on time are suppressed in all subsequent equations. The unknown fields are the scattered pressure field in the fluid $p^{(s)}(\mathbf{r})$, the scattered displacement field in the solid $\mathbf{u}^{(s)}(\mathbf{r})$, the surface pressure field $p_+(\mathbf{r}')$, and the surface displacement field $\mathbf{u}_-(\mathbf{r}')$. The subscripts + and - are used, respectively, to denote that a field quantity is evaluated on the surface in the limit in which \mathbf{r}' approaches the surface from the volume above and below the surface.

At the fluid-elastic interface, the normal component of the displacement and traction are continuous and the tangential component of the traction vanishes. The equations that follow from these boundary conditions are given by

$$\hat{\mathbf{n}}(\mathbf{r}') \cdot \mathbf{u}_-(\mathbf{r}') = \hat{\mathbf{n}}(\mathbf{r}') \cdot \nabla' p_+(\mathbf{r}') / \lambda^{(1)} k_p^{(1)2}, \quad \boldsymbol{\tau}_-(\mathbf{r}') \cdot \hat{\mathbf{n}}(\mathbf{r}') = -p_+(\mathbf{r}') \hat{\mathbf{n}}(\mathbf{r}'), \quad (1a, b)$$

and

$$\hat{\mathbf{n}}(\mathbf{r}') \times \boldsymbol{\tau}_-(\mathbf{r}') = 0. \quad (1c)$$

The tensor $\boldsymbol{\tau}_-(\mathbf{r}')$ is the stress tensor in the solid evaluated on the surface. The unit vector $\hat{\mathbf{n}}(\mathbf{r}')$ is normal to the surface, has its z component directed in the positive z direction, and is given by

$$\hat{\mathbf{n}}(\mathbf{r}') = (\hat{\mathbf{z}} - \partial_{x'} \xi(x', y') \hat{\mathbf{x}}' - \partial_{y'} \xi(x', y') \hat{\mathbf{y}}') / \sqrt{1 + [\partial_{x'} \xi(x', y')]^2 + [\partial_{y'} \xi(x', y')]^2}. \quad (2)$$

The extended boundary condition or null field hypothesis is applied to the total pressure field in the region $z < h_2$ and to the total displacement field in the region $z > h_1$.

2. HELMHOLTZ-KIRCHHOFF INTEGRAL REPRESENTATION OF FIELDS

The Helmholtz-Kirchhoff integral equation representation of the scattered pressure field in the fluid region $z > h_1$, the scattered displacement field in the solid region $z < h_2$, and the equations that follow when the extended boundary condition is enforced on the total fluid pressure field in the region $z < h_2$ and on the total elastic displacement field in the region $z > h_1$ are given by [7]:

$$\int_s ds' [p_+(\mathbf{r}') \hat{\mathbf{n}}(\mathbf{r}') \cdot \nabla' g_0(\mathbf{r}', \mathbf{r}; \mathbf{k}_p^{(1)}) - \lambda^{(1)} k_p^{(1)2} g_0(\mathbf{r}, \mathbf{r}; \mathbf{k}_p^{(1)}) \hat{\mathbf{n}}(\mathbf{r}') \cdot \mathbf{u}_-(\mathbf{r}')] = \begin{cases} p^{(s)}(\mathbf{r}), & (z > h_1) \\ -p^{(t)}(\mathbf{r}), & (z < h_2) \end{cases} \quad (3a, b)$$

and

$$\int_s ds' \{ -p_+(\mathbf{r}') \hat{\mathbf{n}}(\mathbf{r}') \cdot \vec{\mathbf{G}}_0(\mathbf{r}', \mathbf{r}; \mathbf{k}_p^{(2)}, \mathbf{k}_s^{(2)}) - \mathbf{u}_-(\mathbf{r}') \cdot [\hat{\mathbf{n}}(\mathbf{r}') \cdot \vec{\vec{\Sigma}}_0(\mathbf{r}', \mathbf{r}; \mathbf{k}_p^{(2)}, \mathbf{k}_s^{(2)})] \}$$

$$= \begin{cases} 0, & (z > h_1) \\ \mathbf{u}^{(s)}(\mathbf{r}), & (z < h_2) \end{cases} \quad (4a, b)$$

The field representations given by equations (3) and (4) include the boundary conditions given by equations (1a–c). Equations (3b) and (4a) are the equations that follow from the null field hypothesis. The vectors $\mathbf{r} = x\hat{\mathbf{x}} + y\hat{\mathbf{y}} + z\hat{\mathbf{z}}$ and $\mathbf{r}' = x'\hat{\mathbf{x}}' + y'\hat{\mathbf{y}}' + z'\hat{\mathbf{z}}'$ are, respectively, radius vectors to a field point and to a point on the scattering surface. The quantity $ds' = dx' dy' / \sqrt{1 + [\partial_x \xi(x', y')]^2 + [\partial_y \xi(x', y')]^2}$ and is an infinitesimal area element on the scattering surface. In the Helmholtz–Kirchhoff integral representation of a scalar field, the surface normal is directed out of the scattering volume. However, since the unit normal $\hat{\mathbf{n}}(\mathbf{r}')$ points into the fluid volume, a minus sign is included in equations (3a) and (3b). The quantity $g_0(\mathbf{r}', \mathbf{r}; \mathbf{k}_p^{(1)})$ is the scalar Green function for an unbounded region. The quantities $\vec{\mathbf{G}}_0(\mathbf{r}', \mathbf{r}; \mathbf{k}_p^{(2)}, \mathbf{k}_s^{(2)})$ and $\vec{\vec{\Sigma}}_0(\mathbf{r}', \mathbf{r}; \mathbf{k}_p^{(2)}, \mathbf{k}_s^{(2)})$ are, respectively, the Green displacement dyadic and stress triadic for an unbounded region and are given by

$$\vec{\mathbf{G}}_0(\mathbf{r}', \mathbf{r}; \mathbf{k}_p^{(2)}, \mathbf{k}_s^{(2)}) = (1/\rho^{(2)}\omega^2)[\mathbf{V}'g_0(\mathbf{r}', \mathbf{r}; \mathbf{k}_p^{(2)})\mathbf{V} - \mathbf{V}'g_0(\mathbf{r}', \mathbf{r}; \mathbf{k}_s^{(2)})\mathbf{V} + \vec{\mathbf{I}}\mathbf{V}'^2g_0(\mathbf{r}', \mathbf{r}; \mathbf{k}_s^{(2)})], \quad (5)$$

$$\vec{\vec{\Sigma}}_0(\mathbf{r}', \mathbf{r}; \mathbf{k}_p^{(2)}, \mathbf{k}_s^{(2)}) = \lambda^{(2)}\vec{\mathbf{I}}\mathbf{V}' \cdot \vec{\mathbf{G}}_0(\mathbf{r}', \mathbf{r}; \mathbf{k}_p^{(2)}, \mathbf{k}_s^{(2)}) + \mu^{(2)}[\mathbf{V}'\vec{\mathbf{G}}_0(\mathbf{r}', \mathbf{r}; \mathbf{k}_p^{(2)}, \mathbf{k}_s^{(2)}) + \vec{\mathbf{G}}_0(\mathbf{r}', \mathbf{r}; \mathbf{k}_p^{(2)}, \mathbf{k}_s^{(2)})\mathbf{V}']. \quad (6)$$

Representations of the scalar, dyadic and triadic Green functions, and the surface and scattered fields that appear in equations (3) and (4) are given in the next section.

3. FIELD REPRESENTATIONS

Fundamental to the T-matrix formalism is the representation of various unknown fields in terms of scalar, or when appropriate, vector basis functions. Eigenfunction solutions to the scalar wave equation in spherical, cylindrical, and even prolate spheroidal [8, 9] co-ordinates have been used to represent scalar fields and to construct vector basis functions to represent vector and tensor fields. However, to calculate scattering from an infinite fluid–elastic interface with arbitrary roughness, the most appropriate scalar basis functions are Weyl plane waves and it is convenient to represent vector and tensor fields in terms of rectangular vector basis functions constructed from these plane wave functions. These basis functions are similar to those constructed from Floquet plane waves used to represent fields scattered from periodic surface roughness [10]. Although Weyl plane waves have been used as basis functions to represent scalar fields

scattered from rough surfaces, their use in the construction of vector basis functions has not received as much attention. Therefore, the following is a brief description of the construction and properties of rectangular vector basis functions constructed from Weyl plane waves. To simplify the following discussion, reference to the media in the present problem is suppressed.

3.1. RECTANGULAR BASIS FUNCTIONS

A Weyl plane wave function is a solution to the scalar wave equation in rectangular co-ordinates and for an arbitrary wave vector $\mathbf{K}^{(\pm)}$ is given by

$$\chi(\mathbf{r}; \mathbf{K}^{(\pm)}) = e^{i\mathbf{K}^{(\pm)} \cdot \mathbf{r}} \quad (7)$$

with

$$\mathbf{K}^{(\pm)} = \mathbf{K}_\perp \pm K_z \hat{\mathbf{z}}, \quad \mathbf{K}_\perp = K_x \hat{\mathbf{x}} + K_y \hat{\mathbf{y}}, \quad (8a, b)$$

and

$$K_z = \sqrt{k^2 - K_\perp^2} \Theta(k^2 - K_\perp^2) + i\sqrt{K_\perp^2 - k^2} \Theta(K_\perp^2 - k^2). \quad (8c)$$

These scalar basis functions can be used to represent incoming and outgoing propagating waves as well as evanescent waves.

Since the transverse and longitudinal components of the displacement field propagate with different phase speeds, it is necessary to construct transverse vector basis functions that depend on the wave vector $\mathbf{K}_s^{(\pm)}$ and a longitudinal vector basis function that depends on the p -wave vector $\mathbf{K}_p^{(\pm)}$. The wave vectors $\mathbf{K}_s^{(\pm)}$ and $\mathbf{K}_p^{(\pm)}$ are obtained from equation (8) by using, respectively, $k = k_s$ and $k = k_p$ in equation (8c). Rectangular vector basis functions are constructed from the scalar basis functions in the following manner:

$$\hat{\mathbf{X}}_1(\pm \mathbf{r}; \mathbf{K}_s^{(\pm)}) = (1/K_t) \nabla \times \hat{\mathbf{z}} \chi(\pm \mathbf{r}; \mathbf{K}_s^{(\pm)}) = \pm \hat{\mathbf{e}}_1(\mathbf{K}_s^{(\pm)}) \chi(\pm \mathbf{r}; \mathbf{K}_s^{(\pm)}), \quad (9a)$$

$$\hat{\mathbf{X}}_2(\pm \mathbf{r}; \mathbf{K}_s^{(\pm)}) = (1/k_s K_t) \nabla \times \nabla \times \hat{\mathbf{z}} \chi(\pm \mathbf{r}; \mathbf{K}_s^{(\pm)}) = -\hat{\mathbf{e}}_2(\mathbf{K}_s^{(\pm)}) \chi(\pm \mathbf{r}; \mathbf{K}_s^{(\pm)}), \quad (9b)$$

and

$$\hat{\mathbf{X}}_3(\pm \mathbf{r}; \mathbf{K}_p^{(\pm)}) = (k_p/k_s)^{3/2} (1/k_p) \nabla \chi(\pm \mathbf{r}; \mathbf{K}_p^{(\pm)}) = \pm \hat{\mathbf{e}}_3(\mathbf{K}_p^{(\pm)}) \chi(\pm \mathbf{r}; \mathbf{K}_p^{(\pm)}). \quad (9c)$$

On the right side of equations (9a–9c), the \pm sign in front of the expressions refers to the sign of \mathbf{r} . The vector $\hat{\mathbf{K}}_t = \hat{\mathbf{K}}_s \times \hat{\mathbf{z}}/K_t$ with $K_t = |\mathbf{K}_s \times \hat{\mathbf{z}}|$ is the transverse wave vector so that $\mathbf{K}_s \cdot \hat{\mathbf{K}}_t = \hat{\mathbf{z}} \cdot \mathbf{K}_t = 0$ and $\hat{\mathbf{e}}_1(\mathbf{K}_s^{(\pm)}) = i\hat{\mathbf{K}}_t$, $\hat{\mathbf{e}}_2(\mathbf{K}_s^{(\pm)}) = \hat{\mathbf{K}}_s^{(\pm)} \times \hat{\mathbf{K}}_t$, and $\hat{\mathbf{e}}_3(\mathbf{K}_p^{(\pm)}) = i(k_p/k_s)^{3/2} \hat{\mathbf{K}}_p^{(\pm)}$ are polarization vectors. The normalization of the rectangular basis functions is chosen to provide a simple representation of the Green dyadic.

The inner product of two rectangular vector basis functions is defined in the following manner:

$$\langle \hat{\mathbf{X}}_{\kappa'}(\mathbf{r}; \mathbf{K}'^{(\pm)}) | \hat{\mathbf{X}}_\kappa(\mathbf{r}; \mathbf{K}^{(\pm)}) \rangle = \frac{1}{(2\pi)^2} \int_{-\infty}^{\infty} d\mathbf{r}_\perp \hat{\mathbf{X}}_{\kappa'}^*(\mathbf{r}; \mathbf{K}'^{(\pm)}) \cdot \hat{\mathbf{X}}_\kappa(\mathbf{r}; \mathbf{K}^{(\pm)}) \quad (10)$$

($\kappa, \kappa' = 1-3$).

In equation (10), the symbol * denotes the complex conjugate and $\int_{-\infty}^{\infty} \mathbf{dr}_{\perp} = \int_{-\infty}^{\infty} dx \int_{-\infty}^{\infty} dy$. The inner products of the rectangular vector basis functions are given by

$$\begin{aligned} \langle \hat{\mathbf{X}}_1(\mathbf{r}; \mathbf{K}'_s(\pm)) | \hat{\mathbf{X}}_1(\mathbf{r}; \mathbf{K}_s(\pm)) \rangle &= \langle \hat{\mathbf{X}}_2(\mathbf{r}; \mathbf{K}'_s(\pm)) | \hat{\mathbf{X}}_2(\mathbf{r}; \mathbf{K}_s(\pm)) \rangle \\ &= \delta(\mathbf{K}_{\perp} - \mathbf{K}'_{\perp}) \left\{ \begin{array}{l} 1, \quad K'_{sz} \text{ real} \\ \exp(\mp 2|K'_{sz}|z), \quad K'_{sz} \text{ imag} \end{array} \right\}, \quad (11a) \end{aligned}$$

$$\begin{aligned} \langle \hat{\mathbf{X}}_3(\mathbf{r}; \mathbf{K}'_p(\pm)) | \hat{\mathbf{X}}_3(\mathbf{r}; \mathbf{K}_p(\pm)) \rangle &= \delta(\mathbf{K}_{\perp} - \mathbf{K}'_{\perp}) (k_p/k_s)^3 \\ &\quad \left\{ \begin{array}{l} 1, \quad K'_{pz} \text{ real} \\ \exp(\mp 2|K'_{pz}|z), \quad K'_{pz} \text{ imag} \end{array} \right\}, \quad (11b) \end{aligned}$$

$$\langle \hat{\mathbf{X}}_1(\mathbf{r}; \mathbf{K}'_s(\pm)) | \hat{\mathbf{X}}_2(\mathbf{r}; \mathbf{K}_s(\pm)) \rangle = \langle \hat{\mathbf{X}}_1(\mathbf{r}; \mathbf{K}'_s(\pm)) | \hat{\mathbf{X}}_3(\mathbf{r}; \mathbf{K}_p(\pm)) \rangle = 0, \quad (11c)$$

and

$$\begin{aligned} \langle \hat{\mathbf{X}}_2(\mathbf{r}; \mathbf{K}'_s(\pm)) | \hat{\mathbf{X}}_3(\mathbf{r}; \mathbf{K}_p(\pm)) \rangle &= \mp i \delta(\mathbf{K}_{\perp} - \mathbf{K}'_{\perp}) (k_p/k_s)^{3/2} (\hat{\mathbf{K}}_s(\pm) \times \hat{\mathbf{K}}_p)^* \\ &\quad \cdot \hat{\mathbf{K}}_p(\pm) \exp[\pm i(K_{pz} - K_{sz}^*)]. \quad (11d) \end{aligned}$$

It is important to note that the inner products of the rectangular basis functions given by equations (11a–d) apply only to those functions that have the same sign for the z component of the wave vector. The rectangular vector basis functions for s -waves (p -waves) are orthonormal among themselves and carry unit energy for propagating s -waves (p -waves).

3.2. REPRESENTATION OF SCATTERED AND SURFACE FIELDS

In the following, scalar and rectangular vector basis functions are used to construct representations of the scalar and vector fields that appear in equations (3) and (4). To simplify notation, integration over horizontal wave numbers is indicated by $\int_{-\infty}^{\infty} d\mathbf{K}_{\perp} = \int_{-\infty}^{\infty} dK_x \int_{-\infty}^{\infty} dK_y$, and the wave vectors $\mathbf{K}_{\kappa}^{(\pm)}$ and wave number k_{κ} with $\kappa = 1-3$, are defined in the following manner:

$$\mathbf{K}_{\kappa}^{(2\pm)} = \mathbf{K}_s^{(2\pm)} (\delta_{\kappa,1} + \delta_{\kappa,2}) + \mathbf{K}_p^{(2\pm)} \delta_{\kappa,3} \quad (12a)$$

and

$$\mathbf{K}_{\kappa}^{(2)} = k_s^{(2)} (\delta_{\kappa,1} + \delta_{\kappa,2}) + k_p^{(2)} \delta_{\kappa,3}. \quad (12b)$$

The lower case Greek subscript κ is used in equation (12) and in all subsequent equations to refer to the polarization, wave number, and wave vector of the displacement field, i.e., $\kappa = 1$ and $\kappa = 2$ refer, respectively, to the SH and SV components of the displacement field while $\kappa = 3$ refers to the longitudinal component. Representations of the incident pressure field, scattered and surface pressure and displacement fields are given by

$$p^{(i)}(\mathbf{r}) = \frac{\lambda^{(1)}}{k_p^{(1)}} \frac{1}{(2\pi)^2} \int_{-\infty}^{\infty} d\mathbf{K}_{\perp} p^{(i)}(\mathbf{K}_{\perp}) \chi(\mathbf{r}; \mathbf{K}_p^{(1-)}), \quad (13)$$

$$p^{(s)}(\mathbf{r}) = \frac{\lambda^{(1)}}{k_p^{(1)}} \frac{1}{(2\pi)^2} \int_{-\infty}^{\infty} d\mathbf{K}_{\perp} p^{(s)}(\mathbf{K}_{\perp}) \chi(\mathbf{r}; \mathbf{K}_p^{(1+)}) , \quad (14)$$

$$p_+(\mathbf{r}') = \frac{\lambda^{(1)}}{k_p^{(1)}} \frac{1}{(2\pi)^2} \int_{-\infty}^{\infty} d\mathbf{K}'_{\perp} p(\mathbf{K}'_{\perp}) \chi(\mathbf{r}'_{\perp}; \mathbf{K}'_{\perp}) , \quad (15)$$

$$\begin{aligned} \mathbf{u}^{(s)}(\mathbf{r}) &= \frac{1}{(2\pi)^2} \int_{-\infty}^{\infty} d\mathbf{K}_{\perp} \sum_{\kappa=1}^3 \frac{1}{k_{\kappa}^{(2)2}} u_{\kappa}^{(s)}(\mathbf{K}_{\perp}) \hat{\mathbf{X}}_{\kappa}(\mathbf{r}; \mathbf{K}_{\kappa}^{(2-)}) \\ &= \frac{1}{(2\pi)^2} \int_{-\infty}^{\infty} d\mathbf{K}_{\perp} \sum_{\kappa=1}^3 \frac{(-1)^{\kappa+1}}{k_{\kappa}^{(2)2}} u_{\kappa}^{(s)}(\mathbf{K}_{\perp}) \hat{\mathbf{e}}_{\kappa}(\mathbf{K}_{\kappa}^{(2-)}) \chi(\mathbf{r}; \mathbf{K}_{\kappa}^{(2-)}) , \end{aligned} \quad (16)$$

and

$$\begin{aligned} \mathbf{u}_-(\mathbf{r}') &= \frac{1}{(2\pi)^2} \int_{-\infty}^{\infty} d\mathbf{K}'_{\perp} \sum_{\kappa'=1}^3 \frac{1}{k_{\kappa'}^{(2)2}} u_{\kappa'}(\mathbf{K}'_{\perp}) \hat{\mathbf{X}}_{\kappa'}(\mathbf{r}'_{\perp}; \mathbf{K}'_{\perp}) \\ &= \frac{1}{(2\pi)^2} \int_{-\infty}^{\infty} d\mathbf{K}'_{\perp} \sum_{\kappa'=1}^3 \frac{(-1)^{\kappa'+1}}{k_{\kappa'}^{(2)2}} u_{\kappa'}(\mathbf{K}'_{\perp}) \hat{\mathbf{e}}_{\kappa'}(\mathbf{K}'_{\perp}) \chi(\mathbf{r}'_{\perp}; \mathbf{K}'_{\perp}) \end{aligned} \quad (17)$$

The quantities $p^{(l)}(\mathbf{K}_{\perp})$, $p^{(s)}(\mathbf{K}_{\perp})$, $p(\mathbf{K}'_{\perp})$, $u_{\kappa}^{(s)}(\mathbf{K}_{\perp})$ and $u_{\kappa'}(\mathbf{K}'_{\perp})$ are the unknown spectral amplitudes. The factor $\lambda^{(1)}/k_p^{(1)}$ is introduced so that the pressure field spectral amplitudes have the same dimension as the displacement field spectral amplitudes.

In the following, representations of the scalar and tensor Green functions are given for arbitrary media and reference to the various media in the present problem is temporarily suppressed. The representation of the scalar Green function is given by

$$\begin{aligned} g_0(\mathbf{r}', \mathbf{r}; \mathbf{k}) &= \frac{i}{8\pi^2} \int_{-\infty}^{\infty} d\mathbf{K}_{\perp} \frac{\chi(-\mathbf{r}'; \mathbf{K}^{(\pm)}) \chi(\mathbf{r}; \mathbf{K}^{(\pm)})}{K_z} \\ &= \frac{1}{(2\pi)^2} \int_{-\infty}^{\infty} d\mathbf{K}_{\perp} g_0(\mathbf{K}) \chi(-\mathbf{r}'; \mathbf{K}^{(\pm)}) \chi(\mathbf{r}; \mathbf{K}^{(\pm)}) , \quad (z \lesssim z') , \end{aligned} \quad (18a)$$

with

$$g_0(\mathbf{K}) = (i/2)/K_z . \quad (18b)$$

The representation of the Green dyadic is given by

$$\begin{aligned}\vec{\mathbf{G}}_0(\mathbf{r}', \mathbf{r}; \mathbf{k}_p, \mathbf{k}_s) &= \frac{i}{8\pi^2} \frac{k_s}{\mu} \int_{-\infty}^{\infty} d\mathbf{K}_{\perp} \sum_{\kappa=1}^3 \frac{1}{k_{\kappa}} \frac{1}{K_{\kappa z}} \hat{\mathbf{X}}_{\kappa}(-\mathbf{r}'; \mathbf{K}_{\kappa}^{(\pm)}) \hat{\mathbf{X}}_{\kappa}(\mathbf{r}; \mathbf{K}_{\kappa}^{(\pm)}) \\ &= \frac{1}{(2\pi)^2} \int_{-\infty}^{\infty} d\mathbf{K}_{\perp} \sum_{\kappa=1}^3 \vec{\mathbf{G}}_{0\kappa}(\mathbf{K}_{\kappa}^{(\pm)}) \chi(-\mathbf{r}'; \mathbf{K}_{\kappa}^{(\pm)}) \chi(\mathbf{r}; \mathbf{K}_{\kappa}^{(\pm)}), \quad (z \leq z'),\end{aligned}\tag{19a}$$

with

$$\vec{\mathbf{G}}_{0\kappa}(\mathbf{K}_{\kappa}^{(\pm)}) = -(i/2)(-1)^{\kappa+1}(1/\mu)(k_s/k_{\kappa}K_{\kappa z})\hat{\mathbf{e}}_{\kappa}(\mathbf{K}_{\kappa}^{(\pm)})\hat{\mathbf{e}}_{\kappa}(\mathbf{K}_{\kappa}^{(\pm)})\tag{19b}$$

and the Green triadic is given by

$$\begin{aligned}\vec{\vec{\mathbf{S}}}_0(\mathbf{r}', \mathbf{r}; \mathbf{k}_p, \mathbf{k}_s) &= \frac{i}{8\pi^2} \frac{k_s}{\mu} \int_{-\infty}^{\infty} d\mathbf{K}_{\perp} \sum_{\kappa=1}^3 \left\{ \frac{\lambda}{k_p K_{pz}} \vec{\mathbf{I}}\mathbf{V}' \cdot \hat{\mathbf{X}}_3(-\mathbf{r}'; \mathbf{K}_p^{(\pm)}) \delta_{\kappa,3} \right. \\ &\quad \left. + \frac{\mu}{k_{\kappa}} \frac{1}{K_{\kappa z}} [\mathbf{V}' \hat{\mathbf{X}}_{\kappa}(-\mathbf{r}'; \mathbf{K}_{\kappa}^{(\pm)}) + \hat{\mathbf{X}}_{\kappa}(-\mathbf{r}'; \mathbf{K}_{\kappa}^{(\pm)}) \mathbf{V}'] \right\} \hat{\mathbf{X}}_{\kappa}(\mathbf{r}; \mathbf{K}_{\kappa}^{(\pm)}), \quad (z \leq z').\end{aligned}\tag{20}$$

4. MATRIX EQUATIONS

To obtain a system of equations for the spectral amplitudes of the scattered fields in terms of the spectral amplitudes of the surface fields, the representations of the various scalar and tensor fields are used in the Helmholtz–Kirchhoff representations of the scattered fields, equations (3a) and (4b), and the results are used to evaluate the inner products $\langle \chi(\mathbf{r}; \mathbf{K}_p^{(1+)}) | p^{(s)}(\mathbf{r}) \rangle$, $\langle \hat{\mathbf{X}}_1(\mathbf{r}; \mathbf{K}_s^{(2-)}) | \nabla \times \mathbf{u}(\mathbf{r}) \rangle$, $\langle \hat{\mathbf{X}}_2(\mathbf{r}; \mathbf{K}_s^{(2-)}) | \nabla \times \mathbf{u}(\mathbf{r}) \rangle$ and $\langle \chi(\mathbf{r}; \mathbf{K}_p^{(2-)}) | \nabla \cdot \mathbf{u}(\mathbf{r}) \rangle$. A system of equations for the spectral amplitudes of the surface fields is obtained by performing similar operations with the null field equations (3b) and (4a). The results of these calculations are given by

$$\begin{aligned}\frac{1}{(2\pi)^2} \int_{-\infty}^{\infty} d\mathbf{K}_{\perp} \left[\sum_{\kappa'=1}^3 V_{\kappa\kappa'}^{(\pm)}(\mathbf{K}_{\perp}, \mathbf{K}'_{\perp}) u_{\kappa'}(\mathbf{K}_{\perp}) + V_{\kappa 4}^{(\pm)}(\mathbf{K}_{\perp}, \mathbf{K}'_{\perp}) p(\mathbf{K}'_{\perp}) \right] \\ = \begin{cases} 0, & (z > h_1) \\ u_{\kappa}^{(s)}(\mathbf{K}_{\perp}), & (z < h_2) \end{cases}, \quad (21a, b)\end{aligned}$$

and

$$\frac{1}{(2\pi)^2} \int_{-\infty}^{\infty} d\mathbf{K}'_{\perp} \left[\sum_{\kappa'=1}^3 V_{4\kappa'}^{(\mp)}(\mathbf{K}_{\perp}, \mathbf{K}'_{\perp}) u_{\kappa'}(\mathbf{K}'_{\perp}) + V_{44}^{(\mp)}(\mathbf{K}_{\perp}, \mathbf{K}'_{\perp}) p(\mathbf{K}'_{\perp}) \right] = \begin{cases} p^{(s)}(\mathbf{K}_{\perp}), & (z > h_1) \\ -p^{(l)}(\mathbf{K}_{\perp}), & (z < h_2) \end{cases}, \quad (22a, b)$$

The matrix elements $V_{\gamma\gamma'}^{(\pm)}(\mathbf{K}_{\perp}, \mathbf{K}'_{\perp})$ ($\gamma, \gamma' = 1-4$) are given by

$$V_{\kappa\kappa'}^{(\pm)}(\mathbf{K}_{\perp}, \mathbf{K}'_{\perp}) = \mathbf{g}_{0\kappa}(\mathbf{K}_{\kappa}^{(2\pm)}) \cdot [\hat{\mathbf{e}}_{\kappa'}(\mathbf{K}_{\kappa'}^{(2+)}) \cdot \hat{\mathbf{v}}_{\kappa\kappa'}^{(p)}(\mathbf{K}_{\kappa}^{(2\pm)})] \cdot \mathbf{v}^{(g)}(\mathbf{K}_{\kappa}^{(2\pm)}, \mathbf{K}'_{\perp}),$$

$$(\gamma = \kappa = 1-3, \gamma' = \kappa' = 1-3), \quad (23a)$$

$$V_{\kappa 4}^{(\pm)}(\mathbf{K}_{\perp}, \mathbf{K}'_{\perp}) = \mathbf{g}_{0\kappa}(\mathbf{K}_{\kappa}^{(2\pm)}) \cdot [v_{\kappa 4}^{(p)} \mathbf{v}^{(g)}(\mathbf{K}_{\kappa}^{(2\pm)}, \mathbf{K}'_{\perp})], \quad (\gamma = \kappa = 1-3, \gamma' = 4), \quad (23b)$$

$$V_{4\kappa}^{(\pm)}(\mathbf{K}_{\perp}, \mathbf{K}'_{\perp}) = g_0(\mathbf{K}_p^{(1\mp)}) \hat{\mathbf{e}}_{\kappa'}(\mathbf{K}_{\kappa'}^{(2+)}) \cdot [v_{4\kappa}^{(p)} \mathbf{v}^{(g)}(\mathbf{K}_p^{(1\mp)}, \mathbf{K}'_{\perp})],$$

$$(\gamma = 4, \gamma' = \kappa' = 1-3), \quad (23c)$$

and

$$V_{44}^{(\pm)}(\mathbf{K}_{\perp}, \mathbf{K}'_{\perp}) = g_0(\mathbf{K}_p^{(1\mp)}) v_{44}^{(p)}(\mathbf{K}_p^{(1\mp)}) \cdot \mathbf{v}^{(g)}(\mathbf{K}_p^{(1\mp)}, \mathbf{K}'_{\perp}), \quad (\gamma = 4, \gamma' = 4). \quad (23d)$$

The sign convention for the matrix elements $V_{\gamma\gamma'}^{(\pm)}(\mathbf{K}_{\perp}, \mathbf{K}'_{\perp})$ is chosen so that the matrix of coefficients of the null field equations is $\mathbf{V}^{(+)}(\mathbf{K}_{\perp}, \mathbf{K}'_{\perp})$ and the matrix of coefficients for the scattered field equations is $\mathbf{V}^{(-)}(\mathbf{K}_{\perp}, \mathbf{K}'_{\perp})$. It is important to note that the displacement field in the elastic solid and the pressure field scattered from its surface propagate in opposite directions so that the scattered displacement field depends on the wave vector $\mathbf{K}_{\kappa}^{(2-)}$ while the scattered pressure field depends on the wave vector $\mathbf{K}_p^{(1+)}$ so that $\mathbf{V}^{(-)}(\mathbf{K}_{\perp}, \mathbf{K}'_{\perp})$ depends on $\mathbf{K}_{\kappa}^{(2-)}$ and $\mathbf{K}_p^{(1+)}$. The quantity $\mathbf{g}_{0\kappa}(\mathbf{K}_{\kappa}^{(2\pm)})$ is the vector propagator for the κ component of the displacement field and is given by

$$\mathbf{g}_{0\kappa}(\mathbf{K}_{\kappa}^{(2\pm)}) = (-1)^{\kappa+1} \vec{\mathbf{G}}_{0\kappa}(\mathbf{K}_{\kappa}^{(2\pm)}) \cdot \hat{\mathbf{e}}_{\kappa}^*(\mathbf{K}_{\kappa}^{(2\pm)}). \quad (24)$$

The quantity $\mathbf{v}^{(g)}(\mathbf{K}^{(\pm)}, \mathbf{K}'_{\perp})$ is the geometric or rough surface vertex function and is defined by

$$\mathbf{v}^{(g)}(\mathbf{K}^{(\pm)}, \mathbf{K}'_{\perp}) = \int_{-\infty}^{\infty} d\mathbf{r}'_{\perp} [\hat{\mathbf{z}}' - \nabla'_{\perp} \xi(\mathbf{r}')] e^{-i(\mathbf{K}_{\perp} - \mathbf{K}'_{\perp}) \cdot \mathbf{r}'_{\perp}} e^{\mp i K_z \xi(\mathbf{r}'_{\perp})}. \quad (25)$$

Although the form of the roughness profile function has not been given, $\mathbf{v}^{(g)}(\mathbf{K}^{(\pm)}, \mathbf{K}'_{\perp})$ can be expressed in a more convenient form. The Fourier transform of the rough surface phase $e^{\mp i K_z \xi(\mathbf{r}'_{\perp})}$ is given by

$$e^{\mp i K_z \xi(\mathbf{r}'_{\perp})} = \frac{1}{(2\pi)^2} \int_{-\infty}^{\infty} d\mathbf{K}'_{\perp} C(\mathbf{K}'_{\perp}, \pm K_z) e^{i\mathbf{K}'_{\perp} \cdot \mathbf{r}'_{\perp}}, \quad (26a)$$

with

$$C(\mathbf{K}'_{\perp}, \pm K_z) = \int_{-\infty}^{\infty} d\mathbf{r}'_{\perp} e^{-i[\mathbf{K}'_{\perp} \cdot \mathbf{r}'_{\perp} \pm K_z \xi(\mathbf{r}'_{\perp})]}. \quad (26b)$$

From equation (26a), it follows that

$$\int_{-\infty}^{\infty} d\mathbf{r}'_{\perp} \nabla'_{\perp} \xi(\mathbf{r}') e^{-i[\mathbf{K}'_{\perp} \cdot \mathbf{r}'_{\perp} \pm K_z \xi(\mathbf{r}'_{\perp})]} = \mp \frac{\mathbf{K}'_{\perp}}{K_z} C(\mathbf{K}'_{\perp}, K_z). \quad (27)$$

When equations (26) and (27) are used in equation (25), the geometric vertex function is given by

$$\mathbf{v}^{(g)}(\mathbf{K}^{(\pm)}, \mathbf{K}'_{\perp}) = \begin{cases} \mathbf{v}^{(gk)}(\mathbf{K}^{(\pm)}, \mathbf{K}'_{\perp}) C(\mathbf{K}_{\perp} - \mathbf{K}'_{\perp}, \pm K_z), & (K_z \neq 0), \\ -i[(K_x - K'_x)\hat{\mathbf{x}}' + (K_y - K'_y)\hat{\mathbf{y}}'] \xi(\mathbf{K}_{\perp} - \mathbf{K}'_{\perp}) \\ + (2\pi)^2 \delta^2(\mathbf{K}_{\perp} - \mathbf{K}'_{\perp}) \hat{\mathbf{z}}', & (K_z = 0) \end{cases}. \quad (28a)$$

with

$$\mathbf{v}^{(gk)}(\mathbf{K}^{(\pm)}, \mathbf{K}'_{\perp}) = \pm [(K_x - K'_x)\hat{\mathbf{x}}' + (K_y - K'_y)\hat{\mathbf{y}}' \pm K_z \hat{\mathbf{z}}'] / K_z. \quad (28b)$$

For a planar surface or equivalently when $K_z = 0$, $\mathbf{v}^{(g)}(\mathbf{K}^{(\pm)}, \mathbf{K}'_{\perp})|_{\xi(\mathbf{r}'_{\perp})=0} = (2\pi)^2 \delta^2(\mathbf{K}_{\perp} - \mathbf{K}'_{\perp}) \hat{\mathbf{z}}'$ so that the quantities in the matrix elements $V_{\gamma\gamma'}^{(\pm)}(\mathbf{K}_{\perp}, \mathbf{K}'_{\perp})$ with a superscript (p) are vertex functions for scattering from a planar fluid–elastic interface. (Explicit expressions for the planar vertex functions and the matrix elements $V_{\gamma\gamma'}^{(\pm)}(\mathbf{K}_{\perp}, \mathbf{K}'_{\perp})$ are given in Appendix A.) Therefore, the vertices for scattering from a rough fluid–elastic interface are products of two vertex functions; a geometric vertex function that is similar to the two dimensional Fourier transform of the surface normal and a vertex function for scattering from a planar fluid–elastic interface. The geometric vertex function does not depend on the polarization of the surface or scattered fields nor does it contain any term that can produce mode conversion. The expression for the geometric vertex function shows that the rough surface phase term alters the phase of the scatter from that of the planar surface scatter and that the kinematic term produced by the surface derivative causes scattering out of the plane of incidence. Mode conversion is produced by the planar vertex functions.

Although the form of equations (21) and (22) is typical for the null field T-matrix formalism, the representation of the matrix elements given by equation (23) is not. Typically, the matrix elements are expressed in terms of spatial integrals of complicated functions of the basis functions and although such representations are adequate to obtain a numerical solution, they obscure some of the physics of the scattering process. Although for numerical purposes, the representation of matrix elements in terms of vertices and propagators may not be any more advantageous than standard representations, it reveals some of the details of the scattering process: the matrix elements are products of propagators, planar vertex functions, and geometric vertex functions.

In general, the expressions for the surface field spectral amplitudes have a complicated dependence on the various vertices and propagators that appear in equations (21a) and (22b). However, if the null field hypothesis is not used and the equations for the scattered fields are evaluated on the surface and iterated, this problem is avoided and the terms corresponding to the n th iteration are expressed entirely in terms of the vertices and propagators that appear in equations (21b) and (22a) and the incident pressure field. In this paper, it is shown that the T-matrix for an arbitrary perturbation order may be expressed entirely in terms of the elements of a T-matrix density for a planar interface and the rough surface vertex, and that this form of the T-matrix leads to an iterative representation of the perturbation series that may be represented by diagrams that provide a simple and intuitive description of the scattering process.

5. PERTURBATIVE REPRESENTATION OF THE T-MATRIX FOR SCATTERING FROM A ROUGH FLUID-ELASTIC INTERFACE

In this section, a procedure similar to that used previously [1, 11, 12] is used to construct a perturbative representation of the T-matrix for the rough fluid-elastic interface. It is assumed that the spectral amplitudes of the scattered fields can be expressed in the following manner:

$$u_{\kappa}^{(s)}(\mathbf{K}_{\perp}) = \frac{1}{(2\pi)^2} \int_{-\infty}^{\infty} d\mathbf{K}'_{\perp} T_{\kappa}(\mathbf{K}_{\perp}, \mathbf{K}'_{\perp}) p^{(i)}(\mathbf{K}'_{\perp}) \tag{29a}$$

and

$$p^{(s)}(\mathbf{K}_{\perp}) = \frac{1}{(2\pi)^2} \int_{-\infty}^{\infty} d\mathbf{K}'_{\perp} T_4(\mathbf{K}_{\perp}, \mathbf{K}'_{\perp}) p^{(i)}(\mathbf{K}'_{\perp}). \tag{29b}$$

Then it is assumed that perturbative representations of the T-matrices $T_{\gamma}(\mathbf{K}_{\perp}, \mathbf{K}'_{\perp})$ ($\gamma = 1-4$) exist and that they and the surface field spectral amplitudes and the elements of the T-matrix may be represented as power series in hk_{γ} :

$$T_{\gamma}(\mathbf{K}_{\perp}, \mathbf{K}'_{\perp}) = \sum_{n=0}^{\infty} \frac{(hk_{\gamma})^n}{n!} t_{\gamma 4}^{(n)}(\mathbf{K}_{\perp}, \mathbf{K}'_{\perp}), \tag{30}$$

$$u_{\kappa'}(\mathbf{K}'_{\perp}) = \sum_{m'=0}^{\infty} \frac{(hk_{\kappa'}^{(2)})^{m'}}{m'!} u_{\kappa'}^{(m')}(\mathbf{K}'_{\perp}), \quad p(\mathbf{K}'_{\perp}) = \sum_{m'=0}^{\infty} \frac{(hk_p^{(1)})^{m'}}{m'!} p^{(m')}(\mathbf{K}'_{\perp}), \tag{31, 32}$$

and

$$V_{\gamma\gamma'}^{(\pm)}(\mathbf{K}_{\perp}, \mathbf{K}'_{\perp}) = \sum_{m'=0}^{\infty} (hk_{\gamma})^{m'} v_{\gamma\gamma'}^{(\pm)}(\mathbf{K}_{\perp}, \mathbf{K}'_{\perp}) v^{(g,m')}(\mathbf{K}_{\gamma}^{(\pm)}, \mathbf{K}'_{\perp}), \tag{33a}$$

with

$$v^{(g,m)}(\mathbf{K}^{(\pm)}, \mathbf{K}'_{\perp}) = [-i\hat{\mathbf{K}}^{(\pm)} \cdot \hat{\mathbf{z}}]^m / m! \tilde{\xi}^{(m)}(\mathbf{K}_{\perp} - \mathbf{K}'_{\perp}), \tag{33b}$$

and

$$\tilde{\xi}^{(m)}(\mathbf{K}'_{\perp}) = \left. \begin{cases} (2\pi)^2 \delta^2(\mathbf{K}'_{\perp}), & (m = 0), \\ \frac{1}{(2\pi)^{2m-2}} \int_{-\infty}^{\infty} d\mathbf{Q}_{\perp}^{[1]} \int_{-\infty}^{\infty} d\mathbf{Q}_{\perp}^{[2]} \cdots \int_{-\infty}^{\infty} d\mathbf{Q}_{\perp}^{[m]} \\ \xi(\mathbf{Q}_{\perp}^{[1]}) \xi(\mathbf{Q}_{\perp}^{[2]}) \cdots \xi(\mathbf{Q}_{\perp}^{[m]}) \delta_2(-\mathbf{K}'_{\perp} + \mathbf{Q}_{\perp}^{[1]} + \mathbf{Q}_{\perp}^{[2]} + \cdots + \mathbf{Q}_{\perp}^{[m]}), & (m \neq 0) \end{cases} \right\}. \quad (33c)$$

The quantity $v^{(g,m)}(\mathbf{K}_{\gamma}^{(\pm)}, \mathbf{K}'_{\perp})$ is the m th order geometric vertex function and is obtained by expanding the Fourier transform of the rough surface phase $C(\mathbf{K}_{\perp} - \mathbf{K}'_{\perp}, \pm K_z)$ in an infinite series. The quantity $\tilde{\xi}(\mathbf{r}'_{\perp}) = \xi(\mathbf{r}'_{\perp})/h$ and $\tilde{\xi}^{(m)}(\mathbf{K}'_{\perp})$ is the Fourier transform of the m th power of the roughness profile function. The wave vector $\mathbf{K}_{\gamma}^{(\pm)} = K_{\kappa}^{(2\pm)} \delta_{\gamma,\kappa} + \mathbf{K}_p^{(1\pm)} \delta_{\gamma,4}$ and, similarly, the wave number $k_{\gamma} = k_{\kappa}^{(2)} \delta_{\gamma,\kappa} + k_p^{(1)} \delta_{\gamma,4}$.

To obtain representations of the T-matrices $t_{\gamma 4}^{(m)}(\mathbf{K}_{\perp}, \mathbf{K}'_{\perp})$, the perturbative representations of the scattered field spectral amplitudes obtained by using equation (30) in equation (29), the perturbative representations of the surface field amplitudes given by equations (31) and (32), and the perturbative representation of the matrix elements $V_{\gamma\gamma'}^{(\pm)}(\mathbf{K}_{\perp}, \mathbf{K}'_{\perp})$ given by equation (33) are used in the system of equations for the scattered field spectral amplitudes of equations (21) and (22). Then the resulting equations are evaluated for each order of $(hk)^n$. Since quantities that appear in zeroth order perturbation theory form the basis for the perturbative formalism, zeroth order perturbation theory is considered in detail. First, it is important to note that when the arguments of the matrix elements $v_{\gamma\gamma'}^{(\pm)}(\mathbf{K}_{\perp}, \mathbf{K}'_{\perp})$ differ, $v_{\gamma\gamma'}^{(\pm)}(\mathbf{K}_{\perp}, \mathbf{K}'_{\perp}) \neq 0$, however, if $\mathbf{K}_{\perp} = \mathbf{K}'_{\perp}$, $v_{1\bar{1}}^{(\pm)}(\mathbf{K}_{\perp}, \mathbf{K}_{\perp}) = v_{1\bar{1}}^{(\pm)}(\mathbf{K}_{\perp}, \mathbf{K}_{\perp}) = 0$ for $\gamma, \gamma' \neq 1$. Therefore, the SH component of the displacement field is completely decoupled from the other fields and is not excited in zeroth order perturbation theory.

The zeroth order T-matrices are given by

$$t_{\gamma 4}^{(0)}(\mathbf{K}_{\perp}, \mathbf{K}'_{\perp}) = \left. \begin{cases} 0, & (\gamma = 1) \\ (2\pi)^2 t_{\gamma 4}^{(-)}(\mathbf{K}_{\perp}, \mathbf{K}'_{\perp}) \delta(\mathbf{K}_{\perp} - \mathbf{K}'_{\perp}) & (\gamma = 2-4) \end{cases} \right\}. \quad (34)$$

The quantities $t_{\gamma 4}^{(-)}(\mathbf{K}_{\perp}, \mathbf{K}'_{\perp})$ are the $\gamma 4$ elements of the zeroth order T-matrix density given by

$$t_{\gamma\gamma'}^{(\pm)}(\mathbf{K}_{\perp}, \mathbf{K}'_{\perp}) = [\vec{\mathbf{v}}^{(\pm)}(\mathbf{K}_{\perp}, \mathbf{K}'_{\perp}) \cdot \vec{\mathbf{v}}^{(+)}(\mathbf{K}'_{\perp}, \mathbf{K}_{\perp})^{-1}]_{\gamma\gamma'}. \quad (35)$$

At zeroth order perturbation theory, $t_{1\bar{4}}^{(-)}(\mathbf{K}_{\perp}, \mathbf{K}_{\perp}) = 0$, however, beyond zeroth order, $t_{1\bar{4}}^{(-)}(\mathbf{K}_{\perp}, \mathbf{K}'_{\perp}) \neq 0$, and it is necessary to consider all the elements

$t_{\gamma\gamma}^{(\pm)}(\mathbf{K}_\perp, \mathbf{K}'_\perp)$. To simplify notation, only dependence on the horizontal wave numbers of the scattered field \mathbf{K}_\perp and the incident field \mathbf{K}'_\perp are listed explicitly as arguments of the elements of the T-matrix, in general however, the matrix elements also depend on the wave numbers $\mathbf{K}_\gamma^{(-)}$ and $\mathbf{K}_\gamma^{(+)}$.

The explicit expressions for $t_{\gamma 4}^{(-)}(\mathbf{K}_\perp, \mathbf{K}_\perp)$ are given by

$$t_{24}^{(-)}(\mathbf{K}_\perp, \mathbf{K}_\perp) = D/(A + B), \quad t_{34}^{(-)}(\mathbf{K}_\perp, \mathbf{K}_\perp) = C/(A + B), \quad (36a, b)$$

$$t_{44}^{(-)}(\mathbf{K}_\perp, \mathbf{K}_\perp) = (A - B)/(A + B), \quad (36c)$$

where

$$A = K_{pz}^{(1)}[(K_{sz}^{(2)} - K_\perp^2)^2 + 4K_\perp^2 K_{sz}^{(2)} K_{pz}^{(2)}], \quad B = (\rho^{(1)}/\rho^{(2)})k_s^{(2)4} K_{pz}^{(2)}, \quad (37a, b)$$

$$C = 2(\rho^{(1)}/\rho^{(2)})(k_s^{(2)}/k_p^{(1)})(k_p^{(2)}/k_s^{(2)})^{3/2} k_s^{(2)2} K_{pz}^{(1)}(K_{sz}^{(2)2} - K_\perp^2), \quad (37c)$$

and

$$D = -4i(\rho^{(1)}/\rho^{(2)})(k_s^{(2)}/k_p^{(1)})k_s^{(2)2} K_{pz}^{(1)} K_{pz}^{(2)} K_\perp. \quad (37d)$$

The resulting expression for $T_4(\mathbf{K}_\perp, \mathbf{K}_\perp)$ agrees with the result given by Brekhovskikh [13] for scattering from a planar fluid–elastic interface. The expressions for $T_2(\mathbf{K}_\perp, \mathbf{K}_\perp)$ and $T_3(\mathbf{K}_\perp, \mathbf{K}_\perp)$ differ from those given by Brekhovskikh since he formulated the problem in terms of scalar potentials rather than the vector displacement field.

To begin the calculation of the n th order T-matrices, a system of equations for the n th order T-matrices in terms of the spectral amplitudes of the surface fields is obtained from the Helmholtz–Kirchhoff equations and a system of equations for the n th order surface field spectral amplitudes is obtained from the null field equations. Then the system of surface field equations is iterated until the n th order surface field spectral amplitudes are expressed in terms of the zeroth order spectral amplitudes. The expressions for the surface field spectral amplitudes are used in the equations for the T-matrices so that the n th order T-matrix is expressed entirely in terms of the elements of the zeroth order T-matrix and all of the orders geometric vertex function $v^{(gm)}(\mathbf{K}^{(\pm)}, \mathbf{K}'_\perp)$ with $m \leq n$. Since the scattered pressure field is generally of principal interest, the expressions for the n th order T-matrices are lengthy and tedious, and the T-matrices for the displacement field spectral amplitudes can be readily obtained by generalizing the T-matrix for the scattered pressure field spectral amplitude, only the n th order T-matrix for the scattered pressure field spectral amplitude $t_{44}^{(n)}(\mathbf{K}_\perp, \mathbf{K}'_\perp)$ was calculated. A recursive form for $t_{44}^{(n)}(\mathbf{K}_\perp, \mathbf{K}'_\perp)$ is given by

$$\begin{aligned} \frac{1}{n!} k_p^{(1)n} t_{44}^{(n)}(\mathbf{K}_\perp, \mathbf{K}'_\perp) &= \mathcal{V}_{44}^{(-,n)}(\mathbf{K}_\perp, \mathbf{K}'_\perp) \\ &+ \frac{1}{(2\pi)^2} \int_{-\infty}^{\infty} d\mathbf{Q}_\perp \sum_{m=0}^{n-1} \frac{1}{m!} k_p^{(1)m} [\tilde{\mathbf{t}}^{(m)}(\mathbf{K}_\perp, \mathbf{Q}_\perp) \cdot \tilde{\mathcal{V}}^{(+,n-m)}(\mathbf{Q}_\perp, \mathbf{K}'_\perp)]_{44}, \end{aligned} \quad (38a)$$

with

$$\mathcal{V}_{\gamma\gamma}^{(\pm,n)}(\mathbf{Q}_\perp, \mathbf{Q}'_\perp) = q_\gamma^n v^{(g,n)}(\mathbf{Q}_\gamma^{(\pm)}, \mathbf{Q}'_\gamma) t_{\gamma\gamma}^{(\pm)}(\mathbf{Q}_\perp, \mathbf{Q}'_\perp). \quad (38b)$$

The wave vector $\mathbf{Q}_\gamma^{(\pm)}$ is defined identical to $\mathbf{K}_\gamma^{(\pm)}$ and is used to indicate wave vectors over which an integration is performed. The symbol \cdot is used to indicate tensor contraction in the following manner:

$$[\mathbf{t}^{(m)}(\mathbf{K}_\perp, \mathbf{Q}_\perp) \cdot \mathcal{V}^{(+,n-m)}(\mathbf{Q}_\perp, \mathbf{K}'_\perp)]_{44} = \sum_{\gamma=1}^4 t_{4\gamma}^{(m)}(\mathbf{K}_\perp, \mathbf{Q}_\perp) \mathcal{V}_{\gamma 4}^{(+,n-m)}(\mathbf{Q}_\perp, \mathbf{K}'_\perp).$$

Equation (38) provides a simple iterative description of the perturbation series and clearly shows that n th order term is expressed entirely in terms of the all n orders of the geometric vertex function and the T-matrix, $t^{(\pm)}(\mathbf{K}_\perp, \mathbf{K}'_\perp)$. For example, using the expression for the zeroth order T-matrices given by equations (34) and (35), it is a simple calculation to show that the first and second order T-matrices, $t_{44}^{(1)}(\mathbf{K}_\perp, \mathbf{K}'_\perp)$ and $t_{44}^{(2)}(\mathbf{K}_\perp, \mathbf{K}'_\perp)$, respectively, are given by

$$\begin{aligned} k_p^{(1)} t_{44}^{(1)}(\mathbf{K}_\perp, \mathbf{K}'_\perp) &= k_p^{(1)} v^{(g,1)}(\mathbf{K}_4^{(-)}, \mathbf{K}'_\perp) t_{44}^{(-)}(\mathbf{K}_\perp, \mathbf{K}'_\perp) \\ &+ t_{4\gamma}^{(-)}(\mathbf{K}_\perp, \mathbf{K}_\perp) k_\gamma v^{(g,1)}(\mathbf{K}_\gamma^{(+)}, \mathbf{K}'_\perp) t_{\gamma 4}^{(+)}(\mathbf{K}_\perp, \mathbf{K}'_\perp), \quad (\gamma \neq 1), \end{aligned} \quad (39a)$$

and

$$\begin{aligned} \frac{1}{2!} k_p^{(1)2} t_{44}^{(2)}(\mathbf{K}_\perp, \mathbf{K}'_\perp) &= k_p^{(1)2} v^{(g,2)}(\mathbf{K}_4^{(-)}, \mathbf{K}'_\perp) t_{44}^{(-)}(\mathbf{K}_\perp, \mathbf{K}'_\perp) \\ &+ t_{4\gamma}^{(-)}(\mathbf{K}_\perp, \mathbf{K}_\perp) k_\gamma^2 v^{(g,2)}(\mathbf{K}_\gamma^{(+)}, \mathbf{K}'_\perp) t_{\gamma 4}^{(+)}(\mathbf{K}_\perp, \mathbf{K}'_\perp) \\ &+ \frac{1}{(2\pi)^2} \int_{-\infty}^{\infty} d\mathbf{Q}_\perp k_p^{(1)} v^{(g,1)}(\mathbf{K}_4^{(-)}, \mathbf{Q}_\perp) t_{4\gamma}^{(-)}(\mathbf{K}_\perp, \mathbf{Q}_\perp) k_\gamma v^{(g,1)}(\mathbf{Q}_\gamma^{(+)}, \mathbf{K}'_\perp) \\ &\times t_{\gamma 4}^{(+)}(\mathbf{Q}_\perp, \mathbf{K}'_\perp) \\ &+ \frac{1}{(2\pi)^2} \int_{-\infty}^{\infty} d\mathbf{Q}_\perp t_{4\gamma}^{(-)}(\mathbf{K}_\perp, \mathbf{K}_\perp) k_\gamma v^{(g,1)}(\mathbf{K}_\gamma^{(+)}, \mathbf{Q}_\perp) \\ &\times t_{\gamma\gamma'}^{(+)}(\mathbf{K}_\perp, \mathbf{Q}_\perp) k_{\gamma'} v^{(g,1)}(\mathbf{Q}_{\gamma'}^{(+)}, \mathbf{K}'_\perp) t_{\gamma' 4}^{(+)}(\mathbf{Q}_\perp, \mathbf{K}'_\perp). \end{aligned} \quad (39b)$$

The iteration process was carried out for $t_{44}^{(n)}(\mathbf{K}_\perp, \mathbf{K}'_\perp)$ and the result is given by

$$\begin{aligned} (1/n!) k_p^{(1)^n} t_{44}^{(n)}(\mathbf{K}_\perp, \mathbf{K}'_\perp) &= \mathcal{V}_{44}^{(-,n)}(\mathbf{K}_\perp, \mathbf{K}'_\perp) \\ &+ \sum_{m_1=1}^n \frac{1}{(2\pi)^2} \int_{-\infty}^{\infty} d\mathbf{Q}_\perp^{[1]} [\tilde{\mathcal{V}}^{(-,n-m_1)}(\mathbf{K}_\perp, \mathbf{Q}_\perp^{[1]}) \cdot \tilde{\mathcal{V}}^{(+,m_1)}(\mathbf{Q}_\perp^{[1]}, \mathbf{K}'_\perp)]_{44} \\ &+ \sum_{m_2=2}^n \sum_{m_1=m_2}^n \frac{1}{(2\pi)^2} \int_{-\infty}^{\infty} d\mathbf{Q}_\perp^{[1]} \frac{1}{(2\pi)^2} \int_{-\infty}^{\infty} d\mathbf{Q}_\perp^{[2]} \\ &\times [\tilde{\mathcal{V}}^{(-,n-m_1)}(\mathbf{K}_\perp, \mathbf{Q}_\perp^{[1]}) \cdot \tilde{\mathcal{V}}^{(+,m_1-m_2+1)}(\mathbf{Q}_\perp^{[1]}, \mathbf{Q}_\perp^{[2]}) \cdot \tilde{\mathcal{V}}^{(-,m_2-1)}(\mathbf{Q}_\perp^{[2]}, \mathbf{K}'_\perp)]_{44} + \dots \\ &+ \sum_{m_{n-1}=n-1}^n \sum_{m_{n-2}=m_{n-1}}^n \dots \sum_{m_1=m_2}^n \frac{1}{(2\pi)^2} \int_{-\infty}^{\infty} d\mathbf{Q}_\perp^{[1]} \frac{1}{(2\pi)^2} \int_{-\infty}^{\infty} d\mathbf{Q}_\perp^{[2]} \dots \end{aligned}$$

$$\begin{aligned}
 & \times \frac{1}{(2\pi)^2} \int_{-\infty}^{\infty} d\mathbf{Q}_{\perp}^{[n-1]} [\tilde{\mathcal{V}}^{\gamma(-,n-m_1)}(\mathbf{K}_{\perp}, \mathbf{Q}_{\perp}^{[1]}) \cdot \tilde{\mathcal{V}}^{\gamma(+,m_1-m_2+1)}(\mathbf{Q}_{\perp}^{[1]}, \mathbf{Q}_{\perp}^{[2]}) \dots \\
 & \times \tilde{\mathcal{V}}^{\gamma(+,m_{n-1}-n+2)}(\mathbf{Q}_{\perp}^{[n-1]}, \mathbf{K}'_{\perp})]_{44} + \frac{1}{(2\pi)^2} \int_{-\infty}^{\infty} d\mathbf{Q}_{\perp}^{[1]} \frac{1}{(2\pi)^2} \int_{-\infty}^{\infty} d\mathbf{Q}_{\perp}^{[2]} \dots \\
 & \times \frac{1}{(2\pi)^2} \int_{-\infty}^{\infty} d\mathbf{Q}_{\perp}^{[n]} [\tilde{\mathcal{V}}^{\gamma(-,0)}(\mathbf{K}_{\perp}, \mathbf{Q}_{\perp}^{[1]}) \cdot \tilde{\mathcal{V}}^{\gamma(+,1)}(\mathbf{Q}_{\perp}^{[1]}, \mathbf{Q}_{\perp}^{[2]}) \dots \tilde{\mathcal{V}}^{\gamma(+,1)}(\mathbf{Q}_{\perp}^{[n]}, \mathbf{K}'_{\perp})]_{44}. \quad (40)
 \end{aligned}$$

This representation of the T-matrix differs from those obtained when integral equations [2] are iterated. When an integral equation is iterated, the surface fields that appear in the integrand are expressed in terms of the field propagators and scattering vertices that appear in the integral equation. Therefore, the T-matrix can be expressed entirely in terms of field propagators and vertices and it can be represented by diagrams that are similar to Feynman diagrams used in perturbative quantum field theory. In the null field T-matrix formalism, the surface fields are obtained as solutions to the null field equations and expressed in terms of the elements of the inverse of a matrix and not by simple products of field propagators and scattering vertices. Therefore the expressions for the T-matrix given by equations (38) and (40) do not contain the field propagators and scattering vertices that appear in the Helmholtz–Kirchhoff integral equations, since it is more convenient and natural to include these quantities together with the complicated expressions for the zeroth order surface field spectral amplitudes (i.e., the wave functions for intermediate fields) in the elements of the T-matrix $t^{(\pm)}(\mathbf{K}_{\perp}, \mathbf{K}'_{\perp})$.

For completeness in the present discussion, it is important to note that in general, perturbative formalisms of scattering from a rough fluid–elastic interface are subject to divergent phenomena when the transverse wave number approaches a Stoneley wave pole. In the formalism described here, this occurs when the determinant $|v^{(+)}(\mathbf{K}_{\perp}, \mathbf{K}'_{\perp})| = 0$ and $t^{(\pm)}(\mathbf{K}_{\perp}, \mathbf{K}'_{\perp})$ is singular. The properties of Stoneley waves are, of course, well known and have been studied in the context of perturbation theory by Dacol and Berman [1].

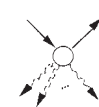


Although the perturbative formalism has been derived for scattering from the rough surface of an elastic solid, it can be extended to include scattering from the rough surface of a rigid and soft surface as well as from the rough surface of a fluid sediment. Scattering from the rough surface of a rigid or soft boundary can be calculated by restricting the indices γ and γ' to 4 and replacing the T-matrix $t_{44}^{(\pm)}(\mathbf{K}_{\perp}, \mathbf{K}'_{\perp})$ by the appropriate free field T-matrix for scattering from a planar surface. Scattering from the rough surface of a fluid sediment can be calculated by restricting γ and γ' to 3 for the fluid sediment and 4 for the upper fluid semi-infinite half space, setting $\mu^{(2)} = 0$, and evaluating the relevant matrix elements in Appendix A. A perturbative T-matrix formalism for scattering from the rough surface of a poroelastic sediment has not been developed. Based on the results here, such a formulation may be obtained by extending the values of the

indices γ and γ' to 5 to include the Biot slow wave in the sediment and replacing the T-matrix for the planar interface by that given by Kargl and Lim [14].

5.1. DIAGRAMMATICS OF PERTURBATION THEORY

To understand the result given by equation (40), it is convenient to represent the T-matrix diagrammatically. Although diagrammatic techniques in acoustic scattering are not new [2, 15–17] and have been developed for scattering from a rough elastic surface by DeSanto [2], the diagrammatic techniques developed here differ from those developed previously. DeSanto considered an elastic half space bounded by a free surface and developed diagrammatic rules to represent the third rank elastic surface Green tensor, its mean and mean square. The fundamental diagrammatic components, a vector propagator, a third rank tensor vertex, a scalar interaction term, and the ensemble average of products of interaction terms, were derived from integral equations for the quantities of interest and then used to represent the Dyson equations. But, the Dyson equation describes a multiple scattering series and not a perturbation series. In the following however, it is shown that the fundamental diagrammatic components developed here are similar to those developed by DeSanto and that the vector propagator in the DeSanto formalism is replaced by the T-matrix $t_{\gamma\gamma'}^{(\pm)}(\mathbf{Q}_\perp, \mathbf{Q}'_\perp)$, the tensor vertex is replaced by the vector vertex $\mathbf{v}^{(gk)}(\mathbf{K}^{(\pm)}, \mathbf{K}'_\perp)$ (equation (A3c)), and the scalar interaction term is replaced by the n th order geometric vertex $v^{(g,m)}(\mathbf{K}_\gamma^{(\pm)}, \mathbf{K}'_\perp)$.

TABLE 1
Fundamental vertices for scattering a fluid pressure wave from a rough elastic surface

Mathematical representation	Graphical representation
1 $v^{(g,m)}(\mathbf{K}_p^{(1\pm)}, \mathbf{K}'_\perp) t_{44}^{(\pm)}(\mathbf{K}_\perp, \mathbf{K}'_\perp)$	$\mathbf{K}_p^{(1-)} \quad \mathbf{K}_p^{(1\pm)}$  $\mathbf{Q}_\perp^{[1]} \mathbf{Q}_\perp^{[2]} \quad \mathbf{Q}_\perp^{[m]}$
2 $v^{(g,m)}(\mathbf{K}_k^{(2\pm)}, \mathbf{K}'_\perp) t_{kk'}^{(\pm)}(\mathbf{K}_\perp, \mathbf{K}'_\perp)$	$\mathbf{K}_p^{(1-)} \quad \mathbf{K}_k^{(2+)}$  $\mathbf{Q}_\perp^{[1]} \mathbf{Q}_\perp^{[2]} \quad \mathbf{Q}_\perp^{[m]}$
3 $v^{(g,m)}(\mathbf{K}_k^{(2+)}, \mathbf{K}'_\perp) t_{kk'}^{(\pm)}(\mathbf{K}_\perp, \mathbf{K}'_\perp)$	$\mathbf{K}_k^{(2+)} \quad \mathbf{K}_k^{(2+)}$  $\mathbf{Q}_\perp^{[1]} \mathbf{Q}_\perp^{[2]} \quad \mathbf{Q}_\perp^{[m]}$

Note: \rightarrow , fluid pressure field; \rightsquigarrow , surface displacement field; \rightsquigarrow , surface fluid pressure field.

TABLE 2

Diagrammatic rules for the construction of a perturbative representation of the T-matrix for scattering a pressure wave from rough fluid–elastic interface

-
- 1 Determine the order of a diagram in the following manner:
 - i. The perturbation order n is given by total number of surface interaction lines.
 - ii. The order of a vertex m is given by the number of surface interaction lines.
 - 2 Construct all diagrams of order n consistent with the allowed vertices.
(Beyond zeroth order, do not include a zeroth order vertex for the incident field.)
 - 3 Include an element of the T-matrix $t^{(\pm)}(\mathbf{K}_\perp, \mathbf{K}'_\perp)$ for each vertex:
 - i. $t_{44}^{(\pm)}(\mathbf{K}_\perp, \mathbf{K}'_\perp)$ for each scalar vertex that contains an incident and ^(surface)_(scattered) fluid pressure field.
 - ii. $t_{4\kappa}^{(\pm)}(\mathbf{K}_\perp, \mathbf{K}'_\perp)$ for each vector that contains an incident surface displacement field and a ^(surface)_(scattered) fluid pressure field.
 - iii. $t_{\kappa 4}^{(\pm)}(\mathbf{K}_\perp, \mathbf{K}'_\perp)$ for each vector that contains an incident fluid pressure field and a ^(surface)_(scattered) surface displacement field.
 - iv. $t_{\kappa\kappa}^{(\pm)}(\mathbf{K}_\perp, \mathbf{K}'_\perp)$ for each tensor vertex that contains an incident displacement field and a ^(surface)_(scattered) displacement field.
 - 4 Include a geometric vertex function $v^{(g,m)}(\mathbf{K}_\perp, \mathbf{K}'_\perp)$ for each m th order vertex.
 - 5 Include a factor $1/(2\pi)^2$ for each interval transverse wave number and integrate over all internal transverse wave numbers.
-

Examination of equation (40) shows that three types of scattering processes occur and that these scattering processes may be described quantitatively by three fundamental scattering functions: (1) a scalar scattering process occurs when the incident and scattered fields are scalar fluid pressure fields and this process is described quantitatively by $\mathcal{V}_{44}^{(\pm,m)}(\mathbf{Q}_\perp, \mathbf{Q}'_\perp)$; (2) vector scattering processes occur when an incident fluid pressure field scatters and mode converts to a displacement field or vice versa and these processes are described quantitatively by $\mathcal{V}_{4\kappa}^{(\pm,m)}(\mathbf{Q}_\perp, \mathbf{Q}'_\perp)$ and $\mathcal{V}_{\kappa 4}^{(\pm,m)}(\mathbf{Q}_\perp, \mathbf{Q}'_\perp)$; (3) a tensor scattering process occurs when a displacement field scatters and mode converts and this process is described by $\mathcal{V}_{\kappa\kappa}^{(\pm,m)}(\mathbf{Q}_\perp, \mathbf{Q}'_\perp)$. Table 1 shows the correspondence between the mathematical expression and graphical representation for each type of scattering process. It is important to note that to simplify the diagrammatics, a single sawtooth line is used to represent any of the three polarization states of the displacement field. However, when scattering from a zeroth order geometric vertex, $t_{\gamma 1}^{(-)}(\mathbf{K}_\perp, \mathbf{K}'_\perp) = t_{1\gamma}^{(-)}(\mathbf{K}_\perp, \mathbf{K}'_\perp) = 0$ for $\gamma \neq 1$ so that the SH field is decoupled completely from the other components of the displacement field and diagrams that include these processes are neglected. Wavy lines are used to indicate the interaction of a displacement field with the rough surface when the geometric vertex function is expressed in terms of the Fourier transform of the rough surface by using equation (33c) in equation (33b). The open circle is used to indicate that the wave numbers of the incident and scattered fields and the transverse wave numbers of the surface interaction are constrained by the delta function that appears in equation (33c). The order of a diagram is given by the total number of surface interaction lines. The rules that determine the manner in which these fundamental functions are

iterated are determined by equation (40) and are summarized in Table 2. Although the scattering functions have been represented diagrammatically by simple point vertices, the expression for $t_{44}^{(-)}(\mathbf{K}_{\perp}, \mathbf{K}'_{\perp})$ given by equation (34) shows that these vertices represent complicated physical processes involving scattering and mode conversion from a planar fluid elastic interface.

Figure 1 shows that diagrammatic representation of the T-matrix through second order perturbation theory. The first diagram of the series is the zeroth order diagram and represents coherent scattering from a planar fluid–elastic interface. The next three diagrams are first order diagrams and represent scattering produced by a single interaction with the rough surface. The first of these diagrams, represents scattering from the surface without excitation of intermediate surface fields. The next two diagrams of the sequence represent scattering in which intermediate surface pressure and displacement fields are excited, propagated, and then scattered from a planar fluid–solid interface. So that even in first order perturbation theory, multiple scattering on the surface occurs. The second order diagrams indicate that there are two types of multiple scattering: (1) multiple scattering between vertices with a single interaction that occurs with excitation and propagation of intermediate surface fields and (2) multiple scattering from a single vertex with multiple surface interactions that occurs without excitation and propagation of intermediate surface pressure and displacement fields. These latter multiple scattering diagrams represent scattering from the rough surface at points that are displaced vertically from the same location in the horizontal plane. The diagrammatic representation of the T-matrix clearly shows that the T-matrix is simply a sum over all possible ways in which all possible intermediate displacement and pressure plane wave fields can mode convert and scatter from the initial to the scattered pressure field.

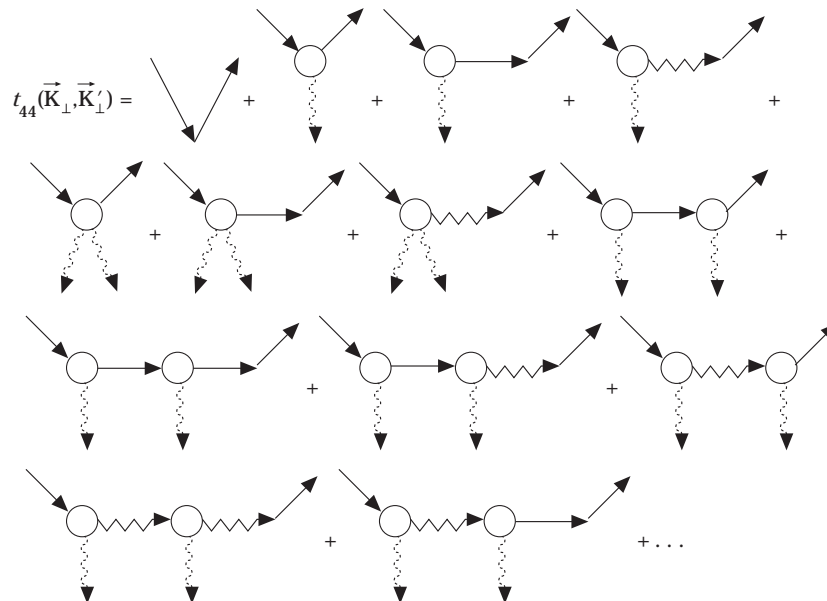


Figure 1. The diagrammatic representation of the T-matrix for scattering a fluid pressure wave from a rough fluid–elastic interface to second order.

6. SCATTERING FROM A FLUID–ELASTIC INTERFACE WITH DOUBLY PERIODIC SINUSOIDAL ROUGHNESS

6.1. ANALYTICAL RESULTS

To investigate the range of validity of the perturbative representation of the T-matrix, it was used to calculate plane wave scattering from a fluid–elastic interface with sinusoidal roughness and the results were compared with those obtained from an exact T-matrix formalism [7]. The incident plane wave and its spectral amplitude are given by

$$p^{(i)}(\mathbf{r}) = p_0 \chi(\mathbf{r}; \mathbf{k}_p^{(1-)}), \quad p^{(i)}(\mathbf{K}_\perp) = (2\pi)^2 p_0 (k_p^{(1)}/\lambda^{(1)}) \delta(\mathbf{K}_\perp - \mathbf{k}_\perp). \quad (41a, b)$$

The roughness profile function is given by

$$\xi(x', y') = a_x \tilde{\xi}(x', y'), \quad (42a)$$

with

$$\tilde{\xi}(x', y') = \sin \mathcal{K}_x x' + (a_y/a_x) \sin \mathcal{K}_y y', \quad (42b)$$

where $a_x(a_y)$ and $A_x(A_y)$ are, respectively, the amplitude and period of the surface roughness in the $x(y)$ directions and $\mathcal{K}_x = 2\pi/A_x$ and $\mathcal{K}_y = 2\pi/A_y$.

When scattering from a surface with periodic roughness, the representation of the scattered fluid pressure field is changed from an integral over Weyl plane waves to a sum over Floquet waves given by [7]

$$p^{(s)}(\mathbf{r}) = \lambda^{(1)} k_p^{(1)} \sum_{\mathbf{m}=-\infty}^{\infty} p_{\mathbf{m}}^{(s)} \chi(\mathbf{r}; \mathbf{k}_{p\mathbf{m}}^{(1+)}), \quad (43)$$

where $p_{\mathbf{m}}^{(s)}$ is the Floquet spectral amplitude and $\chi(\mathbf{r}; \mathbf{k}_{p\mathbf{m}}^{(1+)}) = \exp(\mathbf{k}_{p\mathbf{m}}^{(1+)} \cdot \mathbf{r})$ is a Floquet wave with

$$\mathbf{k}_{\mathbf{m}}^{(\pm)} = k_{xm_x} \hat{\mathbf{x}} + k_{ym_y} \hat{\mathbf{y}} \pm k_{zm} \hat{\mathbf{z}}, \quad k_{xm_x} = k_x + m_x K_x, \quad (44a, b)$$

$$k_{ym_y} = k_y + m_y K_y, \quad k_{zm} = \sqrt{k^2 - k_{xm_x}^2 - k_{ym_y}^2}. \quad (44c, d)$$

In equation (44), the symbol

$$\sum_{\mathbf{m}=-\infty}^{\infty} = \sum_{m_x=-\infty}^{\infty} \sum_{m_y=-\infty}^{\infty}$$

and the index \mathbf{m} denotes the pair of indices (m_x, m_y) , where m_x and m_y are positive or negative integers that specify the order of the Floquet mode. To obtain a perturbative representation for the Floquet spectral amplitudes $p_{\mathbf{m}}^{(s)}$, equations (13), (14), and (29b) are used to construct the perturbative representation of the scattered pressure field for plane wave incidence and then the inner product $\langle p^{(s)}(\mathbf{r}) | \chi(\mathbf{r}; \mathbf{k}_{p\mathbf{m}}^{(1+)}) \rangle$ is evaluated. The perturbative representation of $p_{\mathbf{m}}^{(s)}$ is given by

$$p_{\mathbf{m}}^{(s)} = p_0 \frac{1}{(2\pi)^2} \sum_{n=0}^{\infty} \frac{(a_x k_p^{(1)})^n}{n!} t_{44}^{(n)}(\mathbf{k}_{\mathbf{m}\perp}, \mathbf{k}_\perp). \quad (45)$$

TABLE 3

Floquet spectral amplitudes for the fluid pressure field produced by plane wave scattering from a fluid–solid interface with sinusoidal roughness calculated by non-perturbative and perturbative representations of the T-matrix

T-matrix		Non-perturbative		Perturbative	
m_x	m_y	$\text{real}\{p_{pm}^{(s1+)}\}$	$\text{imag}\{p_{pm}^{(s1+)}\}$	$\text{real}\{p_{pm}^{(s1+)}\}$	$\text{imag}\{p_{pm}^{(s1+)}\}$
0	0	4.11686×10^{-1}	-6.35715×10^{-1}	4.11686×10^{-1}	-6.35715×10^{-1}
0	-1	4.15990×10^{-2}	-1.67066×10^{-2}	4.15979×10^{-2}	-1.67064×10^{-2}
0	-2	1.89504×10^{-3}	-2.73016×10^{-4}	1.89500×10^{-3}	-2.73011×10^{-4}
-1	-1	3.65589×10^{-3}	-5.62204×10^{-4}	3.65582×10^{-3}	-5.62195×10^{-4}
0	-3	5.37038×10^{-5}	-2.13050×10^{-6}	5.40443×10^{-5}	-2.16466×10^{-6}
-1	-2	1.71185×10^{-4}	-1.00159×10^{-5}	1.72213×10^{-4}	-1.00915×10^{-5}
0	-4	7.87494×10^{-7}	-2.21175×10^{-9}	7.90767×10^{-7}	-2.57910×10^{-9}
-1	-3	4.79585×10^{-6}	-8.15469×10^{-8}	4.81936×10^{-6}	-8.26894×10^{-8}
-2	-2	8.00514×10^{-6}	-1.73917×10^{-7}	8.04517×10^{-6}	-1.75434×10^{-7}

An explicit expression for $p_m^{(s)}$ is obtained by using the expression for the geometric vertex function for sinusoidal roughness given in Appendix B in the expression for the T-matrices $t_{44}^{(s)}(\mathbf{k}_{m\perp}, \mathbf{k}_\perp)$ given by equation (40). The final expression for $p_m^{(s)}$ is given in Appendix B. Although the expression for the $p_m^{(s)}$ is very tedious, as a practical matter, perturbation theory is generally used when the perturbation series can be truncated at a relatively low order and terms in the perturbation series are relatively simple to calculate.

6.2. NUMERICAL RESULTS

To be able to determine the effects on scattering of various parameters, a basis set of parameters was chosen and is given by $p_0/(\lambda^{(1)}k_p^{(1)}) = 1$, $k^{(i)} = 10 \text{ m}^{-1}$, $\theta^{(i)} = \phi^{(i)} = 45^\circ$ (the angles $\theta^{(i)}$ and $\phi^{(i)}$ are, respectively, the incident polar and azimuthal angles for the incident plane wave), $a_x = a_y = a = 0.01 \text{ m}$, and $A_x = A_y = A = 2 \text{ m}$, $\rho^{(1)} = 1000 \text{ kg/m}^3$, $c_p^{(1)} = 1493 \text{ m/s}$, $c_p^{(2)} = 2400 \text{ m/s}$, $c_s^{(2)} = 900 \text{ m/s}$, $\rho^{(2)} = 2000 \text{ kg/m}^3$ [18]. In the following discussions, these parameters remain fixed unless specifically noted otherwise.

The non-perturbative representation of $p_m^{(s)}$ given in reference [7] and the perturbative representation of $p_m^{(s)}$ given by equation (B3) to fourth order in the perturbation series were used to evaluate the Floquet spectral amplitudes $p_m^{(s)}$ for propagating modes with m_x and m_y between -2 and 0 . Some of the results of these calculations are shown in Tables 3 and 4 and in Figures 2–4. The numerical calculations were performed simply to indicate that the perturbative formalism can be evaluated and to indicate some regions in which it provides accurate results and not to provide an in depth study of the numerical properties of perturbative rough surface scattering. Extensive numerical results for scattering from a two dimensional fluid–solid interface using a perturbative formalism have been given by Dacol and Berman [1]. Since the non-perturbative representation is used to determine regions in which the perturbative representation is accurate, in the

following discussion it is called the “standard” representation or solution. It is important to note that in all calculations the standard representation was required to satisfy three numerical constraints: (1) energy was required to be conserved to within 0.01, (2) the real and imaginary parts of the spectral amplitudes for the propagating modes $\geq 10^{-5}$ for $|m_x| \leq -3$ and $|m_y| \leq -3$ were required to converge to within 0.01, and (3) the condition number of the matrix of coefficients of the system of linear equations was required to be less than 10^{10} .

Table 3 shows the real and imaginary parts of the $m_x = 0, -1, -2$ and $m_y = 0, -1, -2$ spectral amplitudes of the scattered pressure field in the fluid for the two representations. For the results shown in Table 3, the standard solution required 324 equations, the energy sum was 1.000000 and the condition number of the matrix of coefficients was 12 634.88. The results in Table 3 show that the differences between the real and imaginary parts of the standard and the perturbative representations of the specular mode are extremely small. However, as the order of the modes increases, the difference between the real and imaginary parts of the standard and the perturbative representations of the spectral amplitudes increases: The real and imaginary parts of the perturbative representation of the $m_x = -2, m_y = -2$ spectral amplitude agree with the standard representation to within two significant digits. The fact that the

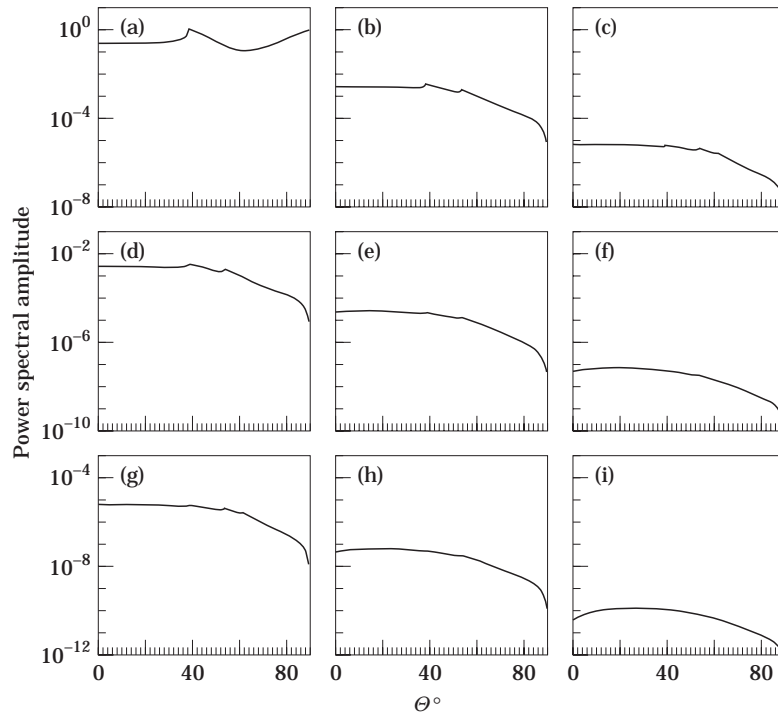


Figure 2. Standard (—) and perturbative (---) representation of the $m_x = 0, -1, -2$ and $m_y = 0, -1, -2$ power spectral amplitudes for pressure field in the fluid versus $\theta = \theta^{(i)}$: (a) $m_x = 0, m_y = 0$; (b) $m_x = -1, m_y = 0$; (c) $m_x = 2, m_y = 0$; (d) $m_x = 0, m_y = -1$; (e) $m_x = -1, m_y = -1$; (f) $m_x = 2, m_y = -1$; (g) $m_x = 0, m_y = -2$; (h) $m_x = -1, m_y = -2$; (i) $m_x = -2, m_y = -2$.

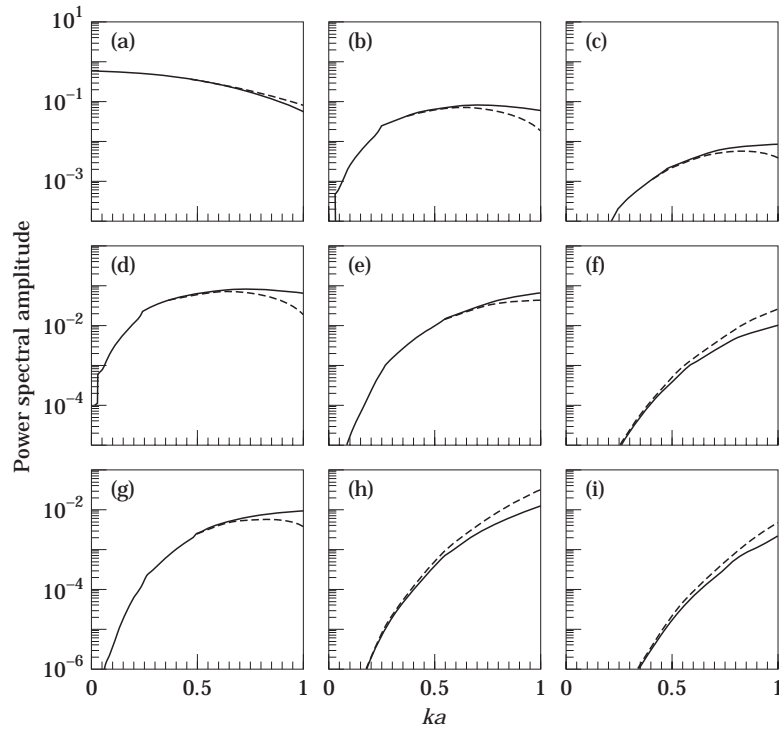


Figure 3. Standard (—) and perturbative (- -) representation of the $m_x=0, -1, -2$ and $m_y=0, -1, -2$ power spectral amplitudes for the fluid pressure field versus ka . Key for (a) to (i) as in Figure 2.

perturbative representation of the spectral amplitudes degrades as the order increases is simply a consequence of the fact that the first contribution to the m th order spectral amplitude does not occur until $n = |m_x| + |m_y|$ and subsequent contributions occur for odd (even) orders only when $|m_x| + |m_y|$ is odd (even), so when the perturbation series is truncated, the number of terms that contributes to the representation of a spectral amplitude decreases as the modal order increases (i.e., the fourth order spectral amplitudes are the result of the single fourth order term in the perturbation series).

Figures 2–4 show, respectively, some of the low order power spectral amplitudes $P_{\rho m}^{(s)} = (k_{\rho z m}^{(1)}/k_{\rho z}^{(1)})|p_m^{(s)}|^2$, for the pressure field scattered in the fluid as functions of $\theta^{(i)}$, the perturbation parameter $k_p^{(1)}a$, and Ka where Ka is the maximum slope of the surface roughness and $K = 2\pi/\lambda$.

Figure 2 shows that for the $m_x = 0, -1$ and $m_y = 0, -1, -2$ power spectral amplitudes, results for the perturbative and standard representations are similar for the standard parameters for all incident angles $\theta^{(i)}$. However, as the following results indicate, this is not a general result.

Figures 3 and 4 show that the difference between the perturbative and standard representations of the $m_x = 0, -1, -2$ and $m_y = 0, -1, -2$ power spectral amplitudes increases with the perturbation parameter $k_p^{(1)}a$ and the surface maximum slope Ka , and that the differences increase with modal order. Figure 4

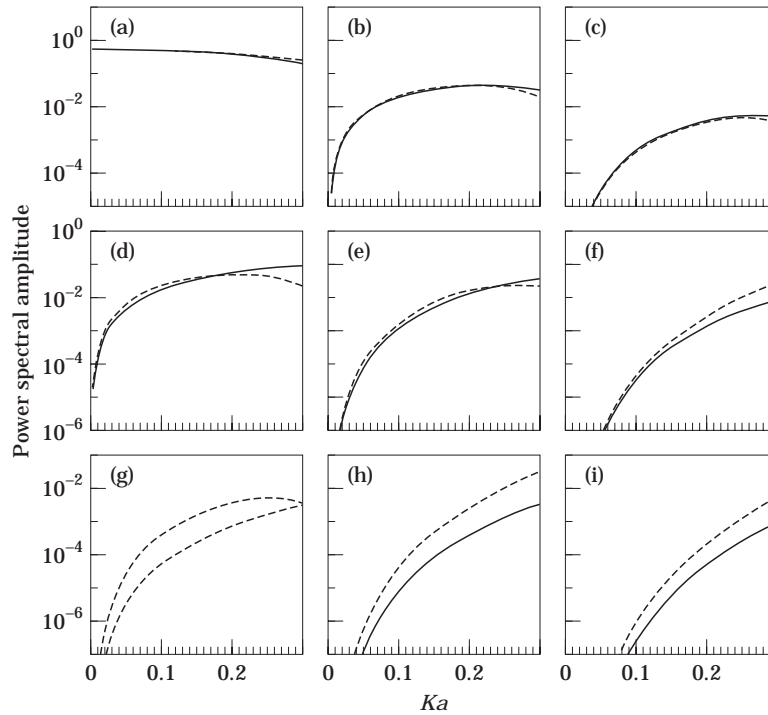


Figure 4. Standard (—) and perturbative (- - -) representations of the $m_x=0, -1, -2$ and $m_y = 0, -1, -2$ power spectral amplitudes for the fluid pressure field versus Ka . Key for (a) to (i) as in Figure 2.

also indicates that the perturbative representation is not only limited to $k_p^{(1)}a < 1$, but also to surface slope $Ka < 0.1$.

Table 4 shows the approximate maximum values of $k_p^{(1)}a$ and Ka for which the perturbative representation of the $m_x = 0, -1, -2$ and $m_y = 0, -1, -2$ power spectral amplitudes differ from the standard representation by less than 5%. The

TABLE 4

Maximum values of $k_p^{(1)}a$ and Ka for which the perturbative representation of the $m_x = 0, -1, -2$ and $m_y = 0, -1, -2$ power spectral amplitudes differ from the standard representation by less than 5%

m_x	m_y	$k_p^{(1)}a$	Ka
0	0	0.80	0.30
0	-1	0.58	0.17
0	-2	0.60	0.18
-1	0	0.58	0.17
-1	-2	0.23	0.07
-2	0	0.60	0.18
-2	-1	0.23	0.07
-2	-2	0.25	0.08

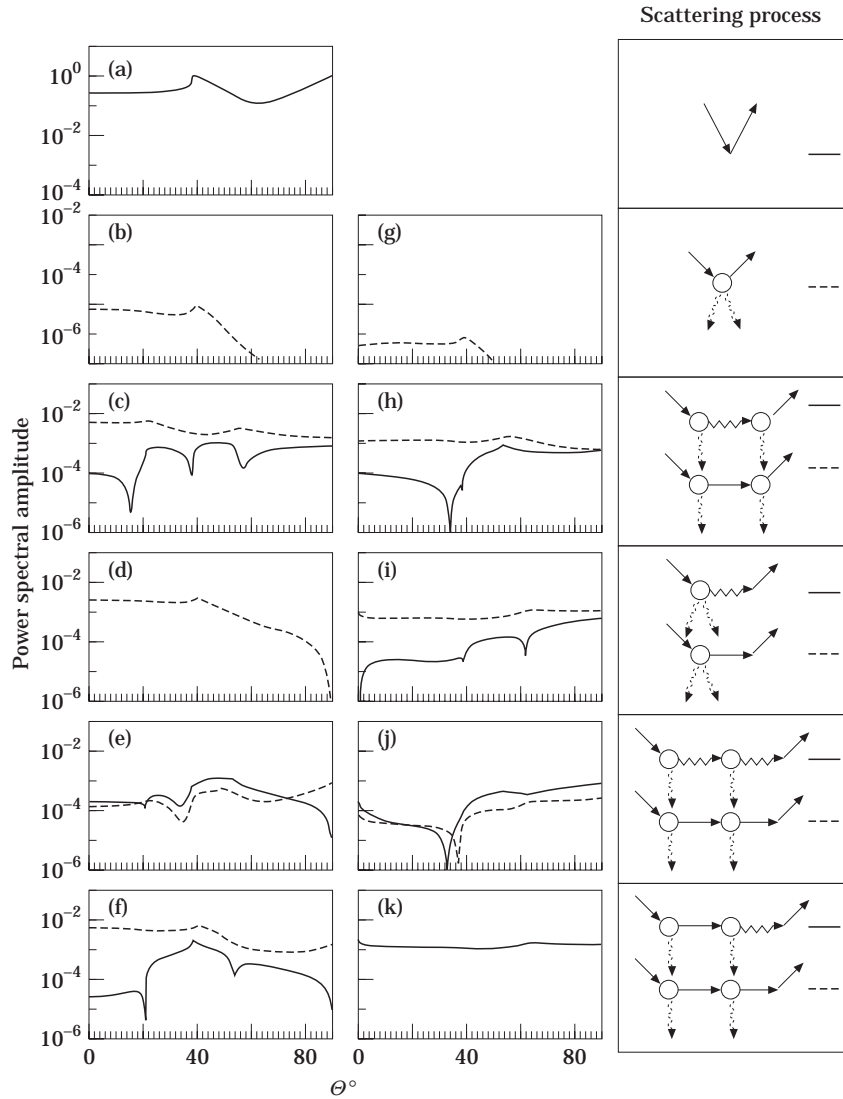


Figure 5. Contributions to the $m_x = m_y = 0$ (left column, (a) to (f)) and $m_x = 0, m_y = -2$ (center column, (g) to (k)). Floquet spectral amplitudes for all zeroth and second order scattering processes for the fluid pressure field as a function of $\theta = \theta^0$.

maximum value of $k_p^{(1)}a$ or Ka for which it may be used is determined by the maximum value of $k_p^{(1)}a$ or Ka for the highest mode required. The maximum value of both parameters decreases as modal order increases.

The failure of the perturbative representation of low order modes as $k_p^{(1)}a$ approaches unity is simply a consequence of the failure of the perturbative assumption and for high spectral orders, the failure of the perturbative representation at lower values of $k_p^{(1)}a$ is, in part, a consequence of truncating the perturbation series.

To illustrate the usefulness of the diagrammatic representation, all scattering processes that occur in the T-matrix to second order and diagrammed in Figure 1

were evaluated and the results for each process were used to calculate power spectral amplitudes as functions of $k_p^{(1)}a = ka$ and $\theta = \theta^{(i)} = \theta^{(f)}$. Some of the results of these calculations are shown in Figures 5–8 for the power spectral amplitudes $P_{0,0}^{(s)}$, $P_{0,-1}^{(s)}$, and $P_{0,-2}^{(s)}$. As noted previously, the first contribution from the perturbation series to the m th order spectral amplitude occurs when $n = |m_x| + |m_y|$ and subsequent contributions occur for odd (even) orders only when $|m_x| + |m_y|$ is odd (even), so that contributions occur for $P_{0,0}^{(s)}$ when $n = 0$ and $n = 2$, for $P_{0,-1}^{(s)}$ when $n = 1$, and for $P_{0,-2}^{(s)}$ when $n = 2$. Figures 5 and 6 show that the various scattering processes exhibit complicated dependence on the incidence angle and that they exhibit derivative discontinuities or scattering “anomalies” characteristic of scattering from periodic surface roughness [19, 20]. In addition, these figures show that the power spectral amplitudes for the purely scalar processes, i.e., processes mediated by surface fluid pressure fields, tend to be greater than vector or tensor processes i.e., processes mediated by surface elastic displacement fields, particularly at low incidence angles. For example consider $P_{0,0}^{(s)}$: Figure 5 shows that the contribution to $P_{0,0}^{(s)}$ from the $n = 0$ scattering process is almost an order of magnitude larger than the largest second order contribution, that the contributions to $P_{0,0}^{(s)}$ from the $n = 2$ scalar processes shown in the third and sixth rows of Figure 5 are bounded by 0.001 and 0.01 for $0^\circ \leq \theta \leq 90^\circ$, and that the contribution from the $n = 2$ scalar process shown in the fourth row of Figure 5 is bounded by 0.001 and 0.01 for $0^\circ \leq \theta \leq 50^\circ$. The power spectral amplitudes for all other $n = 2$ vector and tensor processes are less than ~ 0.001 . Examination of the results for the power spectral amplitudes $P_{0,-1}^{(s)}$ and $P_{0,-2}^{(s)}$ show a similar trend, i.e., contributions to these spectral amplitudes seem to be dominated by purely scalar processes. Comparison of the results shown in Figure 5 with those shown in Figure 3, show that the small peaks observed in the exact results for $P_{0,-1}^{(s)}$ and $P_{0,-2}^{(s)}$ are produced by the purely scalar processes of the perturbative formalism. From a numerical point of view, these results suggest that the elastic effects contained in the reflection coefficient are more important

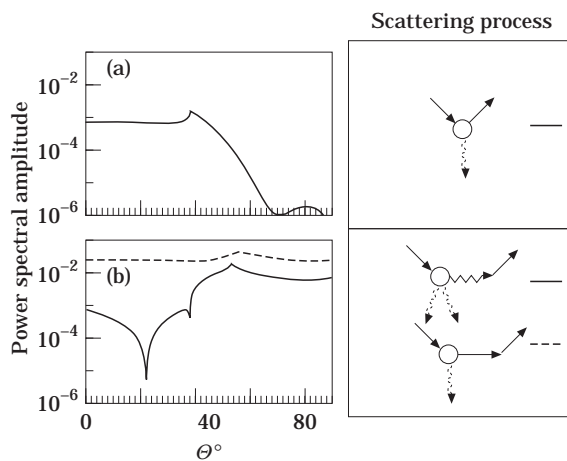


Figure 6. Contributions to the $m_x = 0$, $m_y = -1$ (left column, (a) and (b)) Floquet spectral amplitudes for all first order scattering processes for the fluid pressure field as a function of $\theta = \theta^{(i)}$.

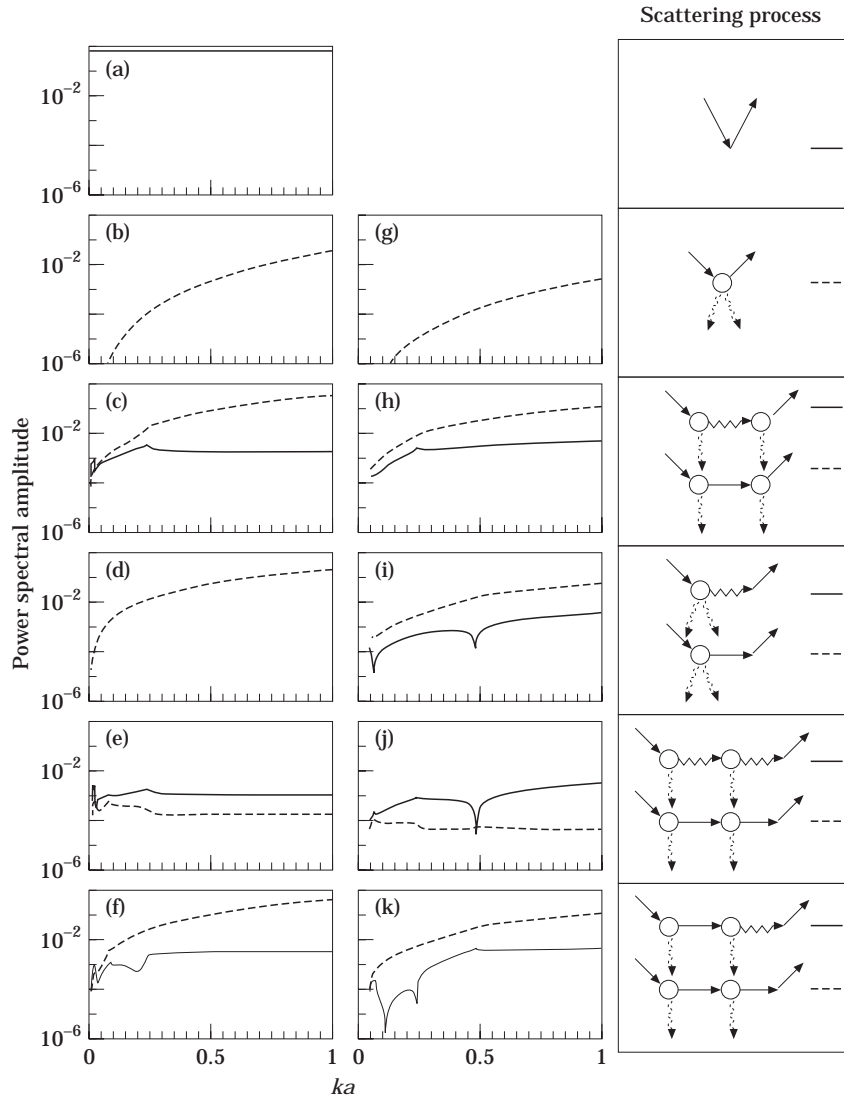


Figure 7. Contributions to the $m_x = m_y = 0$ (left column, (a) to (f)) and $m_x = 0, m_y = -2$ (center column, (g) to (k)) Floquet spectral amplitudes for all zeroth and second order scattering processes for the fluid pressure field as a function of ka .

than those produced by excitation and propagation of surface displacement fields so that the scattering calculation might be simplified by consideration of scalar scattering processes only. However, it is important to emphasize that the results shown in Figures 5 and 6 were obtained for $k_p^{(1)} a = 0.1$ and it is not clear that the dominance of the scalar processes is independent of $k_p^{(1)} a$.

Figures 7 and 8 show contributions to the power spectral amplitudes $P_{0,0}^{(s)}$, $P_{0,-1}^{(s)}$, and $P_{0,-2}^{(s)}$ from the same $n = 0-2$ scattering processes considered in Figures 5 and 6 as functions of ka with $\theta = \theta^{(i)} = \theta^{(l)} = 45^\circ$. These figures show that the contributions to these power spectral amplitudes are dominated by those from the

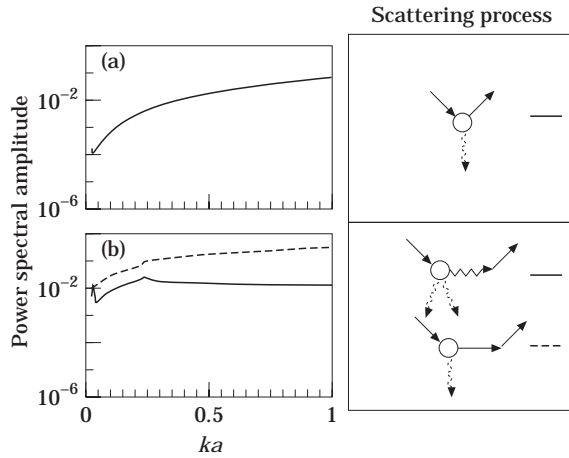


Figure 8. Contributions to the $m_x = 0, m_y = -1$ (left column, (a) and (b)) Floquet spectral amplitudes for all first order scattering processes for the fluid pressure field as a function of ka .

purely scalar processes and the contributions from the purely scalar processes become increasingly dominate as ka increases.

To further examine the extent to which the vector and tensor scattering processes that appear in the perturbation series can be neglected, the perturbation

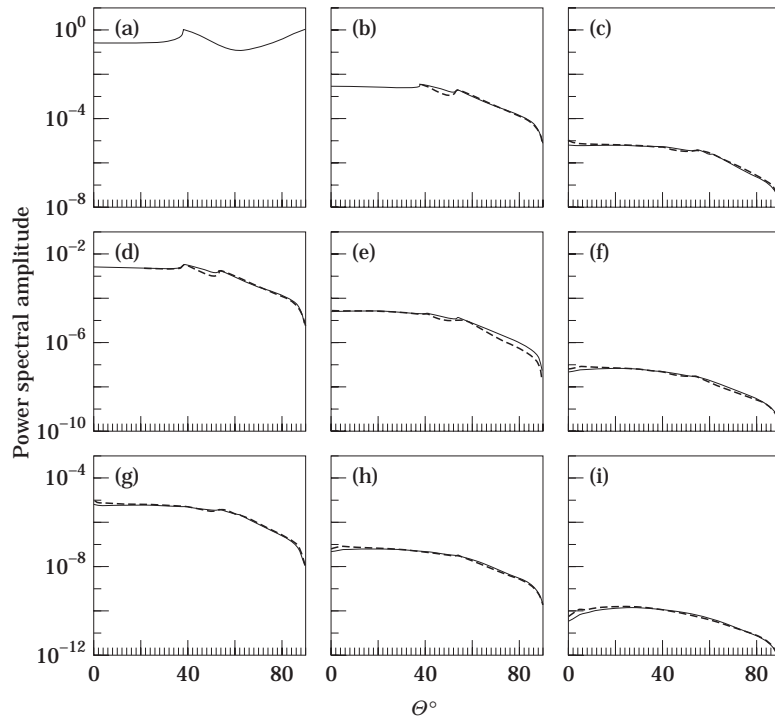


Figure 9. Standard representation (—) and perturbative representation in the “scalar” approximation (- -) of the $m_x = 0, -1, -2$ and $m_y = 0, -1, -2$ power spectral amplitudes for the fluid pressure field versus $\theta = \theta^0$. Key for (a) to (i) as in Figure 2.

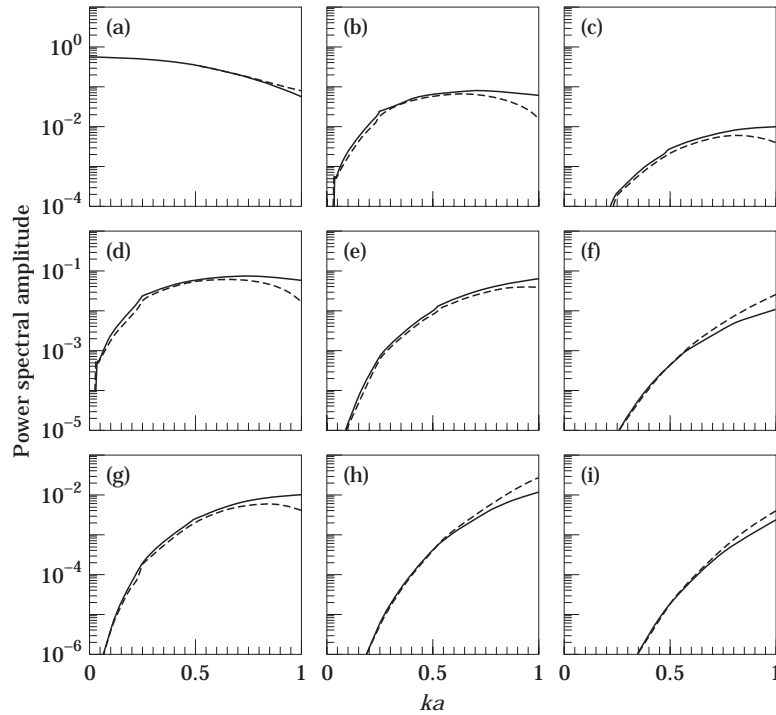


Figure 10. Standard representation (—) and perturbative representation in the “scalar” approximation (---) of the $m_x = 0, -1, -2$ and $m_y = 0, -1, -2$ power spectral amplitudes for the fluid pressure field versus ka . Key for (a) to (i) as in Figure 2.

series to fourth order in the “scalar” approximation in which all vector and tensor scattering processes are neglected, was used to calculate the power spectral amplitudes for $m_x = 0, -1, -2$ and $m_y = 0, -1, -2$ as functions of ka and $\theta = \theta^{(i)}$. Some of the results of these calculations are shown in Figures 9 and 10. These figures show that although the “scalar” approximation is not as accurate as the full perturbation series, it provides surprisingly good results with substantially reduced computational effort over a wide range of angles and ka values. It should be emphasized that the failure of the perturbative results for high ka values is not a failure of the “scalar” approximation, but a more fundamental failure of the perturbative assumption: The results for high ka values might be improved by extending the perturbation series to higher order. In addition, for many purposes and certainly for surfaces with random roughness, the spectral amplitudes are not the quantities of interest. More often, the quantities of interest are the pressure field or, in the case of random surface roughness, the coherent and incoherent components of the scattered field, which depend strongly on the low order terms, i.e., the $n = 0$ and $n = 1$. Figures 9 and 10 suggest that the exact and approximate forms of the power spectral amplitude $P_{0;0}^{(s)}$ are essentially identical over the range $0^\circ \leq \theta \leq 90^\circ$ and $ka \lesssim 0.75$. So that for some purposes the scalar approximation of the perturbation series may provide sufficiently accurate results for substantially reduced computational effort.

7. CONCLUSIONS

It has been shown that the perturbative representation of the T-matrix for scattering a pressure wave from a rough fluid–elastic interface may be calculated by a simple iteration process and expressed entirely in terms of the elements of the T-matrix spectral density for scattering from a planar interface and the geometric vertex function. The representation of the perturbation series in terms of the elements of the planar interface T-matrix spectral density and the geometric vertex function leads to a diagrammatic representation that provides an intuitive understanding of the terms in the rough surface T-matrix, of the physical processes involved, and of the entire process of scattering from rough surfaces: The fields produced by scattering from a rough surface are mediated by excitation of all possible intermediate surface displacement and pressure plane wave fields by mode conversion of all surface fields. Additionally, the diagrams may be used to evaluate the contribution of various types of processes to the entire scattering process. For sinusoidal surface roughness, the perturbative representation was evaluated and compared with a “standard” representation. It was shown that for the physical parameters considered in this paper, the perturbative representation is not only limited to $k_p^{(1)}a < 1$, but also to surface slopes $Ka < 0.1$. In addition, it was shown that purely scalar scattering processes tend to dominate vector and tensor scattering processes and that the “scalar” approximation in which all vector and tensor scattering processes are neglected, provides reasonably accurate results and substantially reduces the computational effort, particularly when the perturbation series is evaluated to high orders.

© US Government 1999

REFERENCES

1. D. K. DACOL and D. H. BERMAN 1988 *Journal of the Acoustical Society of America* **84**, 292–302. Sound scattering from a randomly rough fluid–solid interface.
2. J. A. DESANTO 1973 *Journal of Mathematical Physics* **14**, 1566–1573. Scattering from a random rough surface: Diagram methods for elastic media.
3. M. BLAKEMORE 1986 *Topexpress report, Poseidon House, Castle Park, Cambridge, CB3 0RD, England*. Reflection of acoustic waves from the rough surface of an elastic solid.
4. P. C. WATERMAN 1969 *Journal of the Acoustical Society of America* **45**, 1417–1429. New formulation of acoustic scattering.
5. P. C. WATERMAN 1975 *Journal of the Acoustical Society of America* **57**, 791–802. Scattering by periodic surfaces.
6. P. C. WATERMAN 1976 *Journal of the Acoustical Society of America* **60**, 567–580. Matrix theory of elastic wave scattering.
7. V. VARATHARAJULU and Y. PAO 1976 *Journal of the Acoustical Society of America* **60**, 556–566. Scattering matrix for elastic waves. I. Theory.
8. R. H. HACKMAN 1984 *Journal of the Acoustical Society of America* **75**, 35–45. The transition matrix for acoustic and elastic wave scattering in prolate spheroidal coordinates.
9. R. H. HACKMAN and R. LIM 1994 *Radio Science* **29**, 1035–1049. Development and application of the spheroidal coordinate based T-matrix solution to elastic wave scattering.

10. G. C. BISHOP and J. SMITH 1993 *Journal of the Acoustical Society of America* **94**, 1560–1583. A T-matrix for scattering from a doubly infinite fluid–solid interface with doubly periodic surface roughness.
11. M. NIETO-VESPERINAS and N. GARCIA 1981 *Optica Acta* **28**, 1651–1672. A detailed study of the scattering of scalar waves from random rough surfaces.
12. D. R. JACKSON, D. P. WINEBRENNER and A. ISHIMARU 1988 *Journal of the Acoustical Society of America* **83**, 961–969. Comparison of perturbation theories for rough-surface scattering.
13. L. M. BREKHOVSKIKH 1980 *Waves in Layered Media*. New York, NY: Academic Press; second edition, p. 43.
14. S. G. KARGL and R. LIM 1993 *Journal of the Acoustical Society of America* **94**, 1527–1550. A transition-matrix formulation of scattering in homogeneous, saturated, porous media.
15. K. FURUTSU 1993 *Random Media and Boundaries*. New York: Springer-Verlag; chapter 4.
16. A. G. VORONOVICH 1994 *Wave Scattering from Rough Surfaces*. New York: Springer-Verlag; chapter 5.
17. F. G. BASS and I. M. FUKS 1979 *Wave Scattering from Statistically Rough Surfaces*. New York: Pergamon Press; chapter 11.
18. S. T. MCDANIEL and J. H. BEEBE 1980 *Bottom-Interacting Ocean Acoustics* (edited by W. A. Kuperman and F. B. Jensen). New York: Plenum; p. 501. Propagation over semi consolidated sediments.
19. J. A. DESANTO 1971 *Journal of Mathematical Physics* **12**, 1913–1923. Scattering from a periodic corrugated structure: thin comb with soft boundaries.
20. D. F. MCCAMMON and S. T. MCDANIEL 1986 *Journal of the Acoustical Society of America* **79**, 64–70. Surface reflection: On the convergence of a series to a modified Helmholtz integral equation and the validity of the Kirchhoff approximation.

APPENDIX A: MATRIX ELEMENTS FOR THE FLUID–ELASTIC INTERFACE WITH SURFACE ROUGHNESS

In this appendix, the non-perturbative and perturbative expressions for the matrix elements $V_{\lambda\lambda'}^{(\pm)}(\mathbf{K}_\perp, \mathbf{K}'_\perp)$ are given. The expressions for the planar surface vertex functions are listed below:

$$v_{\kappa\kappa'ijk}^{(p)}(\mathbf{K}_\kappa^{(2\pm)}) = i(-1)^{\kappa'+1}\mu^{(2)}\left(\frac{k_s^{(2)}}{k_\kappa^{(2)}}\right)^2\frac{k_s^{(2)}}{k_\kappa^{(2)}}\left[\delta_{ij}\delta_{k,l} + \delta_{i,l}\delta_{j,k} + \frac{\lambda^{(2)}}{\mu^{(2)}}\delta_{i,k}\delta_{j,l}\delta_{\kappa,3}\right]K_1^{(2\pm)}, \quad (\text{A.1a})$$

$$v_{4\kappa}^{(p)} = (-1)^\kappa k_p^{(1)}(k_p^{(1)}/k_\kappa^{(2)})^2, \quad v_{\kappa 4}^{(p)} = -\lambda^{(1)}(k_s^{(2)}/k_p^{(1)})(k_s^{(2)}/k_\kappa^{(2)})^2 k_\kappa^{(2)}, \quad (\text{A.1b, c})$$

$$v_{44_i}^{(p)}(\mathbf{K}_p^{(1\pm)}) = -K_{p_i}^{(1\pm)}. \quad (\text{A.1d})$$

In equation (A.1), the lower case latin indices refer to the rectangular components of the various quantities.

When the expressions for the various propagators and vertices are used to evaluate the matrix elements $V_{\lambda\lambda'}^{(\pm)}(\mathbf{K}_\perp, \mathbf{K}'_\perp)$, they can be expressed as the product

of the perturbation theory matrix elements $v_{\gamma\gamma'}^{(\pm)}(\mathbf{K}_\perp, \mathbf{K}'_\perp)$ and the Fourier transform of the rough surface phase:

$$V_{\gamma\gamma'}^{(\pm)}(\mathbf{K}_\perp, \mathbf{K}'_\perp) = v_{\gamma\gamma'}^{(\pm)}(\mathbf{K}_\perp, \mathbf{K}'_\perp)C(\mathbf{K}_\perp, \pm K_z), \quad (\text{A.2})$$

with

$$v_{\gamma\gamma'}^{(\pm)}(\mathbf{K}_\perp, \mathbf{K}'_\perp) = \frac{1}{2}(k_\gamma/K_{\gamma z})v_{\gamma\gamma'}^{(\pm)}(\mathbf{K}_\perp, \mathbf{K}'_\perp) \cdot \mathbf{v}^{(gk)}(\mathbf{K}_\gamma^{(\pm)}, \mathbf{K}'_\perp), \quad (\gamma = 1-3, \gamma' = 1-4), \quad (\text{A.3a})$$

and

$$v_{4\gamma'}^{(\pm)}(\mathbf{K}_\perp, \mathbf{K}'_\perp) = \frac{1}{2} \frac{k_p^{(1)}}{K_{pz}^{(1)}} v_{4\gamma'}^{(\pm)}(\mathbf{K}_\perp, \mathbf{K}'_\perp) \cdot \mathbf{v}^{(gk)}(\mathbf{K}_p^{(1\mp)}, \mathbf{K}'_\perp), \quad (\gamma = 4, \gamma' = 1-4), \quad (\text{A.3b})$$

with

$$\mathbf{v}^{(gk)}(\mathbf{K}^{(\pm)}, \mathbf{K}'_\perp) = \pm [(K_x - K'_x)\hat{x}' + (K_y - K'_y)\hat{y}' \pm K_z\hat{z}']/K_z, \quad (\text{A.3c})$$

$$\mathbf{v}_{11}^{(\pm)}(\mathbf{K}_\perp, \mathbf{K}'_\perp) = -[\hat{\mathbf{K}}_t' \cdot \hat{\mathbf{K}}_s \hat{\mathbf{K}}_s^{(2\pm)} + \hat{\mathbf{K}}_t' \cdot \hat{\mathbf{K}}_s^{(2\pm)} \hat{\mathbf{K}}_t], \quad (\text{A.4a})$$

$$\mathbf{v}_{12}^{(\pm)}(\mathbf{K}_\perp, \mathbf{K}'_\perp) = -i[(\hat{\mathbf{K}}_s^{(2+)} \times \hat{\mathbf{K}}_t') \cdot \hat{\mathbf{K}}_t \hat{\mathbf{K}}_s^{(2\pm)} + (\hat{\mathbf{K}}_s^{(2+)} \times \hat{\mathbf{K}}_t') \cdot \hat{\mathbf{K}}_s^{(2\pm)} \hat{\mathbf{K}}_t], \quad (\text{A.4b})$$

$$\mathbf{v}_{13}^{(\pm)}(\mathbf{K}_\perp, \mathbf{K}'_\perp) = -(k_s^{(2)}/k_p^{(2)})^{1/2} [\hat{\mathbf{K}}_p^{(2+)} \cdot \hat{\mathbf{K}}_t \hat{\mathbf{K}}_s^{(2\pm)} + \hat{\mathbf{K}}_p^{(2+)} \cdot \hat{\mathbf{K}}_s^{(2\pm)} \hat{\mathbf{K}}_t], \quad (\text{A.4c})$$

$$\mathbf{v}_{14}^{(\pm)}(\mathbf{K}_\perp, \mathbf{K}'_\perp) = -(\lambda^{(1)}/\mu^{(2)})(k_s^{(2)}/k_p^{(1)})\hat{\mathbf{K}}_t, \quad (\text{A.4d})$$

$$\mathbf{v}_{21}^{(\pm)}(\mathbf{K}_\perp, \mathbf{K}'_\perp) = i[\hat{\mathbf{K}}_t' \cdot (\hat{\mathbf{K}}_s^{(2\pm)} \times \hat{\mathbf{K}}_t)\hat{\mathbf{K}}_s^{(2\pm)} + \hat{\mathbf{K}}_t' \cdot \hat{\mathbf{K}}_s^{(2\pm)}(\hat{\mathbf{K}}_s^{(2\pm)} \times \hat{\mathbf{K}}_t)], \quad (\text{A.4e})$$

$$\begin{aligned} \mathbf{v}_{22}^{(\pm)}(\mathbf{K}_\perp, \mathbf{K}'_\perp) &= -[(\hat{\mathbf{K}}_s^{(2+)} \times \hat{\mathbf{K}}_t') \cdot (\hat{\mathbf{K}}_s^{(2\pm)} \times \hat{\mathbf{K}}_t)\hat{\mathbf{K}}_s^{(2\pm)} \\ &\quad + (\hat{\mathbf{K}}_s^{(2+)} \times \hat{\mathbf{K}}_t') \cdot \hat{\mathbf{K}}_s^{(2\pm)}(\hat{\mathbf{K}}_s^{(2\pm)} \times \hat{\mathbf{K}}_t)], \end{aligned} \quad (\text{A.4f})$$

$$\begin{aligned} \mathbf{v}_{23}^{(\pm)}(\mathbf{K}_\perp, \mathbf{K}'_\perp) &= i(k_s^{(2)}/k_p^{(2)})^{1/2} [\hat{\mathbf{K}}_p^{(2+)} \cdot (\hat{\mathbf{K}}_s^{(2\pm)} \times \hat{\mathbf{K}}_t)\hat{\mathbf{K}}_s^{(2\pm)} \\ &\quad + \hat{\mathbf{K}}_p^{(2+)} \cdot \hat{\mathbf{K}}_s^{(2\pm)}(\hat{\mathbf{K}}_s^{(2\pm)} \times \hat{\mathbf{K}}_t)], \end{aligned} \quad (\text{A.4g})$$

$$\mathbf{v}_{24}^{(\pm)}(\mathbf{K}_\perp, \mathbf{K}'_\perp) = i(\lambda^{(1)}/\mu^{(2)})(k_s^{(2)}/k_p^{(1)})(\hat{\mathbf{K}}_s^{(2\pm)} \times \hat{\mathbf{K}}_t), \quad (\text{A.4h})$$

$$\mathbf{v}_{31}^{(\pm)}(\mathbf{K}_\perp, \mathbf{K}'_\perp) = -(k_p^{(2)}/k_s^{(2)})(k_p^{(2)}/k_s^{(2)})^{3/2} [2\hat{\mathbf{K}}_t' \cdot \hat{\mathbf{K}}_p^{(2\pm)} \hat{\mathbf{K}}_p^{(2\pm)} + (\lambda^{(2)}/\mu^{(2)})\hat{\mathbf{K}}_t'], \quad (\text{A.4i})$$

$$\begin{aligned} \mathbf{v}_{32}^{(\pm)}(\mathbf{K}_\perp, \mathbf{K}'_\perp) &= -i \frac{k_p^{(2)}}{k_s^{(2)}} \left(\frac{k_p^{(2)}}{k_s^{(2)}} \right)^{3/2} [2(\hat{\mathbf{K}}_s^{(2+)} \times \hat{\mathbf{K}}_t') \cdot \hat{\mathbf{K}}_p^{(2\pm)} \hat{\mathbf{K}}_p^{(2\pm)} + \frac{\lambda^{(2)}}{\mu^{(2)}}(\hat{\mathbf{K}}_s^{(2+)} \times \hat{\mathbf{K}}_t')], \end{aligned} \quad (\text{A.4j})$$

$$\mathbf{v}_{33}^{(\pm)}(\mathbf{K}_\perp, \mathbf{K}'_\perp) = -(k_p^{(2)}/k_s^{(2)})^2 [2\hat{\mathbf{K}}_p^{(2+)} \cdot \hat{\mathbf{K}}_p^{(2\pm)} \hat{\mathbf{K}}_p^{(2\pm)} + (\lambda^{(2)}/\mu^{(2)})\hat{\mathbf{K}}_p^{(2+)}], \quad (\text{A.4k})$$

$$\mathbf{v}_{34}^{(\pm)}(\mathbf{K}_\perp, \mathbf{K}'_\perp) = -(\lambda^{(1)}/\mu^{(2)})(k_s^{(2)}/k_p^{(1)})(k_p^{(2)}/k_s^{(2)})^{3/2} \hat{\mathbf{K}}_p^{(2\pm)}, \quad (\text{A.4l})$$

$$\begin{aligned} \mathbf{v}_{41}^{(\pm)}(\mathbf{K}_\perp, \mathbf{K}'_\perp) &= (k_p^{(1)}/k_s^{(2)})^2 \hat{\mathbf{K}}_t', & \mathbf{v}_{42}^{(\pm)}(\mathbf{K}_\perp, \mathbf{K}'_\perp) &= i(k_p^{(1)}/k_s^{(2)})^2 \hat{\mathbf{K}}_s^{(2+)} \times \hat{\mathbf{K}}_t', \end{aligned} \quad (\text{A.4m, n})$$

$$\mathbf{v}_{43}^{(\pm)}(\mathbf{K}_\perp, \mathbf{K}'_\perp) = (k_p^{(1)}/k_p^{(2)})^2 (k_p^{(2)}/k_s^{(2)})^{3/2} \hat{\mathbf{K}}_p^{(2+)}, \quad \mathbf{v}_{44}^{(\pm)}(\mathbf{K}_\perp, \mathbf{K}'_\perp) = \hat{\mathbf{K}}_p^{(1\mp)}. \quad (\text{A.4o, p})$$

APPENDIX B: ANALYTICAL RESULTS FOR SCATTERING FROM
SINUSOIDAL ROUGHNESS

For convenience, it is assumed that $a_x \geq a_y$, then the geometric vertex function is given by

$$\begin{aligned}
 v^{(g,n)}(\mathbf{K}^{(\pm)}, \mathbf{K}'_{\perp}) &= \frac{[-i\hat{\mathbf{K}}^{(\pm)} \cdot \hat{\mathbf{z}}]^n}{n!} \int_{-\infty}^{\infty} d\mathbf{r}'_{\perp} \left[\sin \mathcal{H}_x x' + \frac{a_y}{a_x} \sin \mathcal{H}_y y' \right]^n e^{-i[(K_x - K'_x)x' + (K_y - K'_y)y']} \\
 &= \frac{(2\pi)^2}{(ka_x)^n} \sum_{\ell=0}^{[n]} v_{\ell}^{(g,n)}[\mathbf{K}^{(\pm)}] \delta(K_x - K'_{x\ell}) \delta(K_y - K'_{y\ell}), \tag{B.1}
 \end{aligned}$$

where

$$\begin{aligned}
 v_{\ell}^{(g,n)}[\mathbf{K}^{(\pm)}] &= (-1)^{(n+\ell_x+\ell_y)} (\mathbf{K}^{(\pm)} \cdot \hat{\mathbf{z}} a_x/2)^{n-\ell_z} \\
 &\quad \times (\mathbf{K}^{(\pm)} \cdot \hat{\mathbf{z}} a_y/2)^{\ell_z} (1/\ell_x! (n-\ell_z-\ell_x)! (1/\ell_y! (\ell_z-\ell_y)!), \tag{B.2a}
 \end{aligned}$$

$$K'_{x\ell} = K'_x + (n - \ell_z - 2\ell_x)K_x = k \sin \theta'_{\ell} \cos \phi'_{\ell}, \tag{B.2b}$$

$$K'_{y\ell} = K'_y + (\ell_z - 2\ell_y)K_y = k \sin \theta'_{\ell} \sin \phi'_{\ell}, \tag{B.2c}$$

and

$$K'_{z\ell} = \sqrt{k'^2 - K'^2_{x\ell} - K'^2_{y\ell}}. \tag{B.2d}$$

To simplify writing the geometric vertex function and subsequent expressions, the summation that occurs in equation (B.1) denotes the triple sum given by

$$\sum_{\ell=0}^{[n]} = \sum_{\ell_z=0}^n \sum_{\ell_y=0}^{\ell_z} \sum_{\ell_x=0}^{n-\ell_z}.$$

To derive equation (B.1), the generalized binomial expansion and the complex exponential representation of sine and cosine were used. It is important to note that limits in the sums over ℓ_x and ℓ_y guarantee that the arguments of factorials are always greater than or equal to zero.

The expression for $p_{\mathbf{m}}^{(s)}$ is given by

$$\begin{aligned}
 p_{\mathbf{m}}^{(s)} &= \frac{p_0}{\lambda^{(1)} K_p^{(1)}} \sum_{n=0}^{\infty} \left\{ \sum_{\ell=0}^{[n]} \delta_{n-\ell_z-2\ell_x, m_x} \delta_{\ell_z-2\ell_y, m_y} v_{44;\ell}^{(-,n)}(\mathbf{k}_{\mathbf{p}\mathbf{m}}^{(1+)}, \mathbf{k}_{\perp}) \right. \\
 &\quad \times \sum_{m_1=1}^n \sum_{\ell_1=0}^{[n-m_1]} \sum_{\ell_2=0}^{[m_1]} \delta_{n-\ell_{1z}-\ell_{2z}-2\ell_{1x}-2\ell_{2x}, m_x} \delta_{\ell_{1z}+\ell_{2z}-2\ell_{1y}-2\ell_{2y}, m_y} \\
 &\quad \left. \times v_{47;1;\ell_1}^{(-,n-m_1)}(\mathbf{k}_{\mathbf{p}\mathbf{m}}^{(1+)}, \mathbf{k}_{m_1\ell_{2\perp}}) v_{714;\ell_2}^{(+,m_1)}(\mathbf{k}_{71m_1\ell_2}, \mathbf{k}_{\perp}) \right\}
 \end{aligned}$$

$$\begin{aligned}
 & + \sum_{m_{n-1}=n-1}^n \sum_{m_{n-2}=m_{n-1}}^n \cdots \sum_{m_1=m_2}^n \sum_{\ell_1=0}^{[n-m_1]} \sum_{\ell_2=0}^{[m_1-m_2+1]} \cdots \sum_{\ell_n=0}^{[m_n-1]} \\
 & \times \delta_{n-\ell_{1z}-\ell_{2z}-\cdots-\ell_{nz}-2\ell_{1x}-2\ell_{2x}-\cdots-2\ell_{nx}, m_x} \delta_{\ell_{1z}+\ell_{2z}+\cdots+\ell_{nz}-2\ell_{1y}-2\ell_{2y}-\cdots-2\ell_{2y}, m_y} \\
 & \times v_{4\gamma_1; \ell_1}^{(-, n-m_1)}(\mathbf{k}_{pm}^{(1+)}, \mathbf{k}_{m_1(\ell_2+\ell_3+\cdots+\ell_n)\perp}) \\
 & \times v_{\gamma_1\gamma_2; \ell_2}^{(-, m_1-m_2+1)}(\mathbf{k}_{m_1(\ell_2+\ell_3+\cdots+\ell_n)}, \mathbf{k}_{(m_2-1)(\ell_3+\ell_4+\cdots+\ell_n)\perp}) \\
 & \times v_{\gamma_2\gamma_3; \ell_3}^{(-, m_2-m_3+1)}(\mathbf{k}_{\gamma_2(m_2-1)(\ell_3+\ell_4+\cdots+\ell_n)}, \mathbf{k}_{(m_3-2)(\ell_4+\ell_5+\cdots+\ell_n)\perp}) \\
 & \cdots v_{\gamma_{n-1}\gamma_n; \ell_n}^{(+, m_{n-1})}(\mathbf{k}_{\gamma_{n-1}(m_{n-1})\ell_n}, \mathbf{k}_\perp) \\
 & + \sum_{\ell_2=0}^{[1]} \cdots \sum_{\ell_{n+1}=0}^{[1]} \delta_{n-\ell_{2z}-\cdots-\ell_{nz}-2\ell_{2x}-\cdots-2\ell_{nx}, m_x} \delta_{\ell_{2z}+\cdots+\ell_{nz}-2\ell_{2y}-\cdots-2\ell_{ny}, m_y} \\
 & \times v_{4\gamma_1; 000}^{(-, 0)}(\mathbf{k}_{pm}^{(1+)}, \mathbf{k}_{n(\ell_2+\ell_3+\cdots+\ell_n)\perp}) \\
 & \times v_{\gamma_1\gamma_2; \ell_2}^{(-, 1)}(\mathbf{k}_{n(\ell_2+\ell_3+\cdots+\ell_n)}, \mathbf{k}_{(n-1)(\ell_3+\ell_4+\cdots+\ell_n)\perp}) \\
 & \times v_{\gamma_2\gamma_3; \ell_3}(\mathbf{k}_{\gamma_2(n-1)(\ell_3+\ell_4+\cdots+\ell_n)}, \mathbf{k}_{(n-2)(\ell_4+\ell_5+\cdots+\ell_n)\perp}) \\
 & \cdots v_{\gamma_n\gamma_{n+1}; \ell_{n+1}}^{(+, 1)}(\mathbf{k}_{\gamma_n(\ell_{n+1})}, \mathbf{k}_\perp \}, \tag{B.3a}
 \end{aligned}$$

with

$$v_{\gamma\gamma'; \ell}^{(\pm, m)}(\mathbf{k}_\gamma, \mathbf{k}'_\perp) = v_\ell^{(g, m)}(\mathbf{k}_\gamma) t_{\gamma\gamma'}^{(\pm)}(\mathbf{k}_\perp, \mathbf{k}'_\perp). \tag{B.3b}$$